Effective boundary conditions for second-order homogenization

Manon Thbaut, Basile Audoly, Claire Lestringant

Effective boundary conditions for second-order homogenization

MANON THBAUT
Laboratoire de Mécanique des Solides
CNRS, Institut Polytechnique de Paris
91120 Palaiseau, France

BASILE AUDOLY
Laboratoire de Mécanique des Solides
CNRS, Institut Polytechnique de Paris
91120 Palaiseau, France

CLAIRE LESTRINGANT
Institut Jean Le Rond d'Alembert,
Sorbonne Université, CNRS,
75005 Paris, France

Using matched asymptotic expansions, we derive an equivalent bar model for a periodic, one-dimensional lattice made up of linear elastic springs connecting both nearest and next-nearest neighbors. We obtain a strain-gradient model with effective boundary conditions accounting for the boundary layers forming at the endpoints. It is accurate to second order in the scale separation parameter $\varepsilon \ll 1$, as shown by a comparison with the solution to the discrete lattice problem. The homogenized modulus associated with the gradient effect (gradient stiffness) is found negative, as is often the case in second-order homogenization. Negative gradient stiffnesses are widely viewed as paradoxical as they can induce short-wavelength oscillations in the homogenized solution. In the one-dimensional lattice, the asymptotically correct boundary conditions are shown to suppress the oscillations, thereby restoring consistency. By contrast, most of the existing work on second-order homogenization makes use of postulated boundary conditions which, we argue, not only ruin the order of the approximation but are also the root cause of the undesirable oscillations.

Keywords Elastic lattices, Asymptotic homogenization, Second-order homogenization.

1. INTRODUCTION

The interest in architected materials has grown recently due to advances in fabrication techniques such as additive manufacturing. The complex microstructure of these materials makes their modeling quite challenging. In particular, standard homogenization usually misses significant size-effects. These materials are thus often better described by generalized media, whose constitutive behavior involves either additional degrees of freedom [CC09] or superior gradients of displacement [Ger73; Min64; Tou62]. In this work, we focus on models of the latter kind. Two-scale asymptotic expansion [A77; BP89; BLP11; San80] is a powerful tool to derive such models without requiring ad-hoc kinematic assumptions [Bou20]. When the microstructure is not degenerate, the standard homogenization framework is recovered at leading order. Next, higher orders are shown to lead to strain-gradient contributions [S18a; S18b; Bou96; BS11; GK89; SC00; TB96] which improve the accuracy of the homogenized model.

Solving these higher-order effective models however raises three main issues.

1. These models are of limited accuracy in the boundary regions due to the loss of periodicity near the boundaries [Dum86; San86; YAL24]. Capturing first-order boundary effects appearing in 2D domains [AA99; Dum86] and in 3D composites [FF+22; KMU19], have been shown to increase significantly the quality of the predictions associated with standard homogenization, especially near the boundaries. If neglected, these effects can even lead to unreliable failure criteria in composites [FF+22]. In the context of higher-order homogenization which aims at improving the order of approximation of the solution, capturing these boundary effects is likely to become even more important.
2. Another issue is that the effective equilibrium equation derived from these models is of fourth order and therefore requires additional boundary conditions, compared to the full micro-structural problem. The derivation of such boundary conditions is usually ad-hoc [AMPB08; TB93] and there lacks a rigorous method to obtain asymptotically exact effective boundary conditions up to second order.
3. Finally, higher-order asymptotic homogenization has been reported to yield non-positive strain gradient stiffness for a large number of structures in dimension 1, 2 and 3 [ABV16; AL23; DLSS22; LM18; SC00]. This makes oscillating terms appear in the solution that are not present in the physical system. Moreover, such short-wavelength oscillations are inconsistent with the fundamental assumptions of homogenization theory, which assumes that the macroscopic displacement is smooth. This non-positivity has hindered the wide adoption of strain-gradients models.

In this paper, we analyze the simplest structure that features these difficulties, namely a one-dimensional lattice of springs connecting nearest and next-nearest neighbors. In the absence of next-nearest neighbor interactions, the lattice would become isostatic and homogenization could be bypassed entirely: introducing next-nearest neighbor interactions helps us stay away from this special case. In addition, boundaries break the lattice periodicity in the presence of next-nearest neighbor interactions, causing boundary layers to form. Finally, lattices of this kind are known to lead to a non positive strain-gradient stiffness [KZ64; TB93]: the effective equilibrium equation is found as

$$K u''(x) - \varepsilon^2 B u''''(x) + \bar{f}(x) = 0 \tag{1.1}$$

where u denotes the macroscopic displacement, ε is the microscopic length and $\bar{f}(x)$ is the distributed loading. The leading-order homogenized modulus K is positive, $K>0$, but the higher-order one B is *negative*, $B<0$. The coefficient B will be referred to as the *gradient stiffness*.

The higher-order beam model in (1.1) is said to be 'ill-posed' because of the 'incorrect' sign $B<0$ which makes oscillating terms appear in the solution. Indeed, the homogeneous differential equation $Ku''(x)-\varepsilon^2 Bu''''(x)=0$ has quickly oscillatory solutions of the form $\cos\left(\sqrt{K/(-B)}\,\frac{x}{\varepsilon}+\varphi\right)$ when $B<0$. The coarse-grained equilibrium of a *plain* chain of springs (*i.e.*, without second neighbors) is also of the form (1.1) with a negative gradient stiffness $B=-K/12<0$ as well, ε being then the initial length of the springs. In the context of lattice dynamics, a net force of the form $Ku''(x)-\varepsilon^2 Bu''''(x)$ with $B<0$ is commonly found in the balance of linear momentum, and leads to so-called 'bad' Boussinesq equations [KZ64; Ros86; TB93].

We propose the following approach to address the three issues listed above. It is based on the method of matched asymptotic expansions which can capture boundary effects up to any desired order of approximation [BO99; Eck73; Ili92; Lag88]. We use this approach to smoothly connect an *outer* solution (homogenized solution valid far from the endpoints) to an *inner* solution (boundary layer solution valid near the endpoints). This approach has been applied to derive effective jump conditions that include first order interface effects induced by networks of periodic defects, like inclusions or cracks, inside 3D elastic bodies [ACM98; H74]. Here, we follow [BMP21] in the context of elastic plates and [Vin16] in the context of wave transmission through an interface and push this approach up to second order. We obtain a boundary-value problem consisting of Equation (1.1) with two boundary conditions at each endpoint, representing the boundary layers in an effective way: (*i*) a mixed (Robin-type) condition that extends the standard kinematic relation with a gradient correction and (*ii*) a novel static condition. At leading order, the classical homogenization results are recovered.

We interpret the static boundary condition (*ii*) as a compatibility condition warranting that the solution to the leading-order bar model $Ku''(x)+\bar{f}(x)=0$ gets perturbed *regularly* when the gradient term $-B\varepsilon^2 u''''(x)$ is included. We argue that the solution to the higher-order homogenized model can then be obtained perturbatively by solving a hierarchy of problems $Ku''(x)=\cdots$ for classical elastic bars, the gradient effect entering as a source term in the right-hand side only.

The different flavors of homogenization differ in the following sense. Leading-order homogenization delivers a classical bar model $Ku''(x)+\bar{f}(x)=0$ having one boundary condition at every end, of the kind (*i*). First-order homogenization, accurate to order ε^1 included, delivers the same differential equation with refined boundary conditions of the kind (*i*), which become of Robin type [AA99; Dum86]. Here, we deal with second-order homogenization: the order of the differential equation increases from 2 to 4 due to the new term $-B\varepsilon^2 u''''(x)$ and, concurrently, one additional static boundary condition of the kind (*ii*) appears at each end.

The spring lattice is presented in Section 2. The main features of the matched-asymptotic method are covered in Section 3. The homogenization procedure and an analysis of the boundary layer are presented in Section 4 and 5 respectively. In Section 6, these solutions are matched and effective boundary conditions are obtained. In Section 7, we show that the homogenized problem is amenable to a perturbative solution. Finally, we validate our approach in Section 8, by comparing the solutions to the boundary-value problem to the equilibrium of the discrete lattice, for vanishingly small cell size ε.

2. ONE-DIMENSIONAL, PERIODIC SPRING LATTICE

In this section, we present the one-dimensional lattice which we seek to homogenize.

2.1. Lattice properties

The lattice is sketched in Figure 2.1b. It has a finite length $L=\mathcal{O}(1)$ and a large number of cells, $N\gg 1$. We denote the cell size as

$$\varepsilon=\frac{L}{N}\ll 1$$

and address the homogenization limit $\varepsilon\to 0$ where the number of cells $N=\mathcal{O}(\varepsilon^{-1})$ is large.

The lattice is obtained by replicating the unit cell shown in orange in Figure 2.1a, comprising four different springs with respective spring constants k_1/ε, k_2/ε, k_3/ε and k_4/ε. Having the spring constants scale as $1/\varepsilon$ ensures that the equivalent traction modulus remains finite in the limit $\varepsilon\to 0$. There are two families of nodes (also known as Bravais sub-lattices), denoted as solid (–) versus open (+) symbols in Figure 2.1b. Nodes belonging to the sub-lattice (–) are connected by the long springs with constant k_3/ε, and nodes belonging to the sub-lattice (+) by the long springs with constant k_4/ε. Nodes (–) have a spring with constant k_1/ε on their right-hand side and a spring with constant k_2/ε on their left-hand side, and vice-versa for the nodes (+).

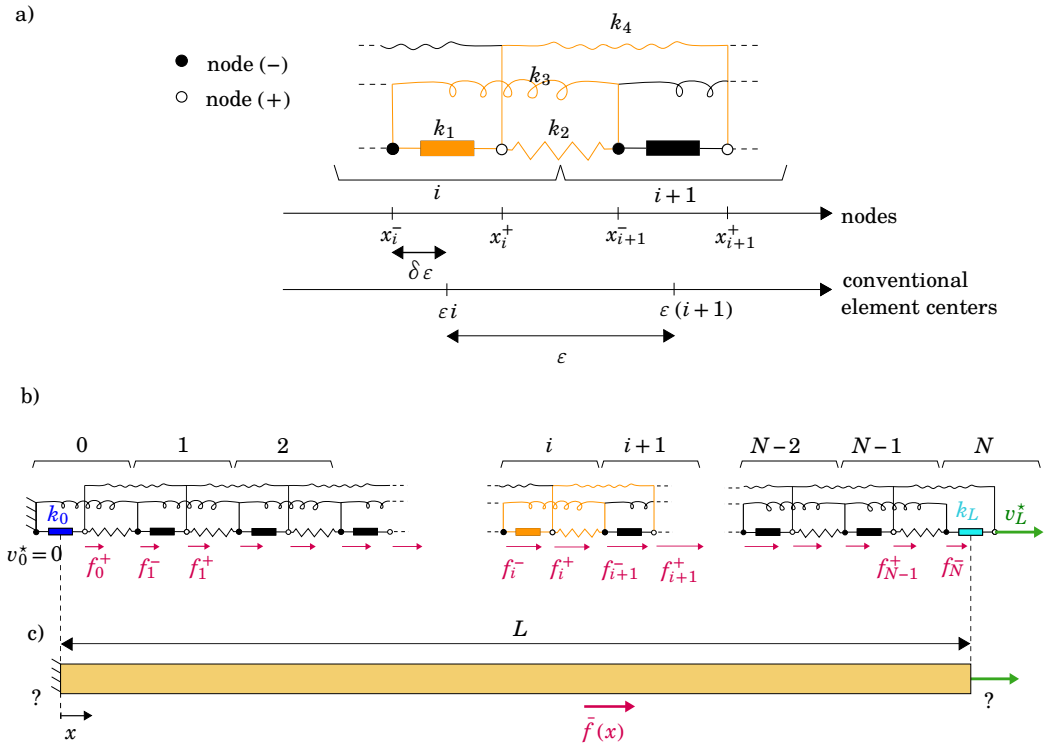

Figure 2.1. A one-dimensional lattice of linear springs. a) Unit cell (orange springs) made up of four types of springs connecting nearest and next-nearest neighbors. b) Full view of the lattice. The terminal springs use 'exceptional' constants k_0 (blue) and k_L (cyan); the displacement of the terminal nodes is prescribed as $v_0^\star$ and $v_L^\star$, with $v_0^\star=0$ here. c) Using higher-order homogenization, we aim at identifying an equivalent bar model (orange) along with the relevant boundary conditions. Note that we have omitted a scaling factor ε^{-1} in all springs constants shown in this figure: the actual spring constants are k_0/ε, k_1/ε, etc.

Remark 2.1. This lattice was designed so as to not fall into any of the two following special cases, in which homogenization can be bypassed entirely: (*i*) lattices possessing a single Bravais sub-lattice, and (*ii*) one-dimensional lattices connecting nearest neighbors only. The special case (*i*) corresponds to $k_3=k_4$ and $k_1=k_2$ and has been solved in [CT02]. The case (*ii*) corresponds to $k_3=k_4=0$, the tension in the remaining springs being given directly by a global balance of forces.

Cells are labelled by an index i in the range $0\leqslant i\leqslant N$. Nodes are indexed by their cell number i and by a sign $\pm$. Their initial position is given by

$$x_i^\pm=\varepsilon\,(i\pm\delta), \tag{2.1}$$

where x is the coordinate along the lattice and

$$\delta=\frac{1}{4}. \tag{2.2}$$

As shown in Figure 2.1b, the terminal springs connecting nearest-neighbors use specific spring constants k_0/ε and k_L/ε.

The *interior* nodes are subjected to a force $f_i^\pm$ which is prescribed in terms of the node initial position via a smooth function $\bar f(x)$ as

$$\begin{aligned} f_i^- &= \frac{\varepsilon}{2}\bar f(x_i^-) && \text{if } 1\leqslant i\leqslant N\\ f_i^+ &= \frac{\varepsilon}{2}\bar f(x_i^+) && \text{if } 0\leqslant i\leqslant N-1 \end{aligned} \tag{2.3}$$

and the *terminal* nodes x_0^- and x_N^+ are subjected to imposed displacements, denoted as $v_0^\star$ and $v_L^\star$, respectively,

$$\begin{aligned} v_0^- &= v_0^\star,\\ v_N^+ &= v_L^\star. \end{aligned} \tag{2.4}$$

In the right-hand sides of (2.3), $\bar f(x)$ represents the applied force per unit length in the continuous limit $\varepsilon\to 0$. The applied force varies slowly, in the sense that its variation from one node to the next $|f_i^+-f_i^-|=\mathcal{O}(\varepsilon^2)$ and $|f_{i+1}^--f_i^+|=\mathcal{O}(\varepsilon^2)$ is much smaller than its magnitude $\mathcal{O}(\varepsilon)$.

2.2. Discrete equilibrium equations

When subjected to nodal forces in (2.3) and to the prescribed displacements in (2.4), the lattice reaches an equilibrium. We denote as $v_i^{\pm}$ the displacement of the node of type $\pm$ in cell i, which occurs along the x-axis in the present one-dimensional setting.

With the aim to obtain the equilibrium of the lattice in compact form, we collect the displacement of the nodes belonging to the cell i ($0 \leqslant i \leqslant N$) into a vector $\boldsymbol{V}_i$ having length 2

$$\boldsymbol{V}_i = \begin{pmatrix} v_i^- \\ v_i^+ \end{pmatrix}. \tag{2.5}$$

The nodal forces in the *interior* cells ($1 \leqslant i \leqslant N-1$) are collected similarly into a vector $\boldsymbol{F}_i$ having length 2,

$$\boldsymbol{F}_i = \begin{pmatrix} f_i^- \\ f_i^+ \end{pmatrix}. \tag{2.6}$$

In view of (2.1) and (2.3), the force $\boldsymbol{F}_i$ in any interior cell ($1 \leqslant i \leqslant N-1$) is given in terms of a smooth function $\overline{\boldsymbol{F}}(x)$ as $\boldsymbol{F}_i = \frac{\varepsilon}{2}\overline{\boldsymbol{F}}_\varepsilon(\varepsilon i)$, where

$$\overline{\boldsymbol{F}}_\varepsilon(x) = \begin{pmatrix} \bar{f}(x-\varepsilon\,\delta) \\ \bar{f}(x+\varepsilon\,\delta) \end{pmatrix}. \tag{2.7}$$

It can be checked that the equilibrium of the nodes takes the form of a discrete boundary-value problem for the cell displacements $\boldsymbol{V}_i$,

$$\begin{cases} \frac{1}{\varepsilon}(\boldsymbol{P}\cdot\boldsymbol{V}_{i+1} + \boldsymbol{Q}\cdot\boldsymbol{V}_i + \boldsymbol{R}\cdot\boldsymbol{V}_{i-1}) + \boldsymbol{F}_i = \boldsymbol{0} \quad \text{for} \quad 1 \leqslant i \leqslant N-1 \\ \frac{1}{\varepsilon}(\boldsymbol{P}_0\cdot\boldsymbol{V}_1 + \boldsymbol{Q}_0\cdot\boldsymbol{V}_0) + \boldsymbol{F}_0 = \boldsymbol{0} \\ \frac{1}{\varepsilon}(\boldsymbol{Q}_N\cdot\boldsymbol{V}_N + \boldsymbol{R}_N\cdot\boldsymbol{V}_{N-1}) + \boldsymbol{F}_N = \boldsymbol{0} \end{cases} \tag{2.8}$$

where the matrices appearing in the equilibrium $(2.8)_1$ of the interior nodes are given by

$$\boldsymbol{P} = \begin{pmatrix} k_3 & 0 \\ k_2 & k_4 \end{pmatrix}, \qquad \boldsymbol{Q} = \begin{pmatrix} -(k_1+k_2+2k_3) & k_1 \\ k_1 & -(k_1+k_2+2k_4) \end{pmatrix}, \qquad \boldsymbol{R} = \begin{pmatrix} k_3 & k_2 \\ 0 & k_4 \end{pmatrix}, \tag{2.9}$$

while those entering in the boundary conditions $(2.8)_{2,3}$ are given by

$$\begin{aligned} \boldsymbol{P}_0 &= \begin{pmatrix} 0 & 0 \\ k_2 & k_4 \end{pmatrix} & \boldsymbol{Q}_0 &= \begin{pmatrix} 1 & 0 \\ k_0 & -(k_0+k_2+k_4) \end{pmatrix} \\ \boldsymbol{Q}_N &= \begin{pmatrix} -(k_L+k_2+k_3) & k_L \\ 0 & 1 \end{pmatrix} & \boldsymbol{R}_N &= \begin{pmatrix} k_3 & k_2 \\ 0 & 0 \end{pmatrix}. \end{aligned} \tag{2.10}$$

In the boundary conditions $(2.8)_{2,3}$, we have extended the force vector $\boldsymbol{F}_i$ to the terminal cells ($i = 0, N$) by defining

$$\boldsymbol{F}_i = \frac{\varepsilon}{2}\overline{\boldsymbol{F}}_\varepsilon(\varepsilon i) + \begin{cases} \boldsymbol{\Delta}_0 & \text{if } i = 0 \\ \boldsymbol{\Delta}_L & \text{if } i = N \\ \boldsymbol{0} & \text{if } 0 < i < N \end{cases} \tag{2.11}$$

with the force exceptions

$$\boldsymbol{\Delta}_0 = \begin{pmatrix} -\frac{v_0^\star}{\varepsilon} - \frac{\varepsilon}{2}\bar{f}(-\varepsilon\,\delta) \\ 0 \end{pmatrix}, \qquad \boldsymbol{\Delta}_L = \begin{pmatrix} 0 \\ -\frac{v_L^\star}{\varepsilon} - \frac{\varepsilon}{2}\bar{f}(\varepsilon(N+\delta)) \end{pmatrix}. \tag{2.12}$$

Remark 2.2. The definition (2.11) of the discrete force coincides with that introduced above Equation (2.7) on *interior* cells, namely $\boldsymbol{F}_i = \frac{\varepsilon}{2}\overline{\boldsymbol{F}}_\varepsilon(\varepsilon i)$. The exceptional contributions in (2.12) applicable to the terminal cells are designed in such a way that Equations $(2.8)_{2,3}$ yield the correct boundary conditions. Consider the conditions $(2.8)_2$ at the left boundary $i = 0$, for instance: with the help of (2.10) and (2.11–2.12–2.7), it can be spelled out as

$$\begin{aligned} \frac{1}{\varepsilon}(v_{\bar{0}}) + \left(\frac{\varepsilon}{2}\bar{f}(\not{\varepsilon}\,\delta) + \left(-\frac{v_0^\star}{\varepsilon} - \frac{\varepsilon}{2}\bar{f}(\not{\varepsilon}\,\delta)\right)\right) &= 0 \\ \frac{1}{\varepsilon}(k_2 v_{\bar{1}} + k_4 v_1^+ + k_0 v_{\bar{0}} - (k_0+k_2+k_4)\,v_0^+) + \frac{\varepsilon}{2}\bar{f}(+\varepsilon\,\delta) &= 0. \end{aligned}$$

The first equation is nothing but the kinematic condition $(2.4)_1$ and the second equation can be rewritten as $(k_2/\varepsilon)\,(v_{\bar{1}} - v_0^+) + (k_4/\varepsilon)\,(v_1^+ - v_0^+) - (k_0/\varepsilon)\,(v_0^+ - v_{\bar{0}}) + \frac{\varepsilon}{2}\bar{f}(+\varepsilon\,\delta) = 0$ which yields the balance of forces on node x_0^+.

In this paper, we consider the values of the elastic constants listed in Table 2.1 by way of illustration. None of the findings reported in this paper depends crucially on these values. In the companion notebook, written in the symbolic calculation language [Wol21] and distributed online [Thb24], symbolic values are used for all spring constants in both the uni cell (k_1, k_2, k_3, k_4) and in the exceptions (k_0, k_L) at the ends.

k_2/k_1	k_3/k_1	k_4/k_1	k_0/k_1	k_L/k_1
3	1	2	1	1

Table 2.1. Numerical values of the spring constants used for numerical illustrations.

3. OVERVIEW AND MAIN RESULTS

In this Section we briefly present the main result of the paper, which is to derive a boundary-value problem for the macroscopic displacement $u_\varepsilon(x)$. By *boundary-value problem*, we mean a differential equation for u along with boundary conditions at both ends. The differential equation can be obtained by standard methods from higher-order homogenization: our main contribution is to derive the asymptotically correct boundary conditions and to highlight the nice properties of the solutions to the associated boundary-value problem.

3.1. Summary of homogenization results

Standard methods of homogenization (see Section 4) deliver the equilibrium of the equivalent bar in the form

$$K u_\varepsilon''(x) - \varepsilon^2 B u_\varepsilon''''(x) + \bar{f}(x) = \mathcal{O}(\varepsilon^3). \tag{3.1}$$

With the particular choice of spring constants in Table 2.1, the traction modulus K and the second-gradient modulus B are given by

$$\begin{aligned} K &= +\frac{15}{4} k_1 > 0, \\ B &= -\frac{9}{32} k_1 < 0. \end{aligned} \tag{3.2}$$

The leading-order $K u_\varepsilon''(x) + \bar{f}(x) = 0$ defines a classical bar model having a positive traction modulus $K > 0$. The higher-order term $-\varepsilon^2 B u_\varepsilon''''(x)$ improves the accuracy of the predictions. The gradient stiffness B happens to be negative, $B < 0$.

The lattice we consider is non-degenerate at the leading order ($K \neq 0$), and therefore does not belong to the special family of lattices, such as pantographs [DLSS22], featuring soft modes ($K = 0$) and a positive gradient modulus ($B > 0$). In non-degenerate structures ($K \neq 0$), by contrast, negative gradient stiffness $B < 0$ is the rule rather than the exception [ABV16; AL23; LM18]. It leads to the following paradoxes:

1. the solutions $u_\varepsilon(x)$ to the differential equation (3.1) feature undesirable, short-wavelength oscillations, see Section 3.2;
2. the homogenized strain energy underpinning the equilibrium equations (3.1) is non-positive, implying that *any* solution $u_\varepsilon(x)$ is unstable.

We leave the resolution of the second paradox to a follow-up paper, where the energy properties of the homogenized model are discussed in depth. Here, we solve the first paradox by showing that the undesirable oscillations are suppressed when mathematically correct boundary conditions are used.

Remark 3.1. The gradient stiffness B is negative for *any* set of values of the spring constants $k_1 > 0, \ldots, k_4 > 0$ and not just for the particular values listed in Table 2.1. Indeed, its general expression, derived in the companion notebook, is

$$B = -k_1 \frac{(q_2+q_3+q_4) + (q_2^2 + 14 q_2 (q_3+q_4) + 12 (q_3-q_4)^2) + q_2 (q_2 (q_3+q_4) + 12 (q_3-q_4)^2)}{48 (1+q_2)^2}, \tag{3.3}$$

where $q_2 = k_2/k_1 > 0$, $q_3 = k_3/k_1 > 0$ and $q_4 = k_4/k_1 > 0$ are the stiffness contrasts.

3.2. *Ad hoc* boundary conditions and their deficiencies

A common trick to equip the homogenized Equation (3.1) with 'sensible' boundary conditions is the following. Multiplying by a test function and integrating by parts, one can show that the equilibrium problem (3.1) is the stationary condition, in the interior of the domain $0 < x < L$, of the energy functional

$$\mathscr{E}_{\text{adhoc}}[u] = \frac{1}{2} \int_0^L \left(K u'^2(x) + \varepsilon^2 B u''^2(x) \right) \mathrm{d}x - \int_0^L \bar{f}(x)\, u(x)\, \mathrm{d}x. \tag{3.4}$$

Assuming that the prescribed displacement at the endpoints can be represented by the kinematic condition $u(0) = v_0^\star$ and $u(L) = v_L^\star$, one then postulates that the equilibrium solution $u_\varepsilon(x)$ makes $\mathscr{E}_{\text{adhoc}}$ stationary in the space of kinematically admissible functions $u(x)$ satisfying $u(0) = v_0^\star$ and $u(L) = v_L^\star$, thereby following a standard pattern in the theory of elasticity. This variational problem delivers the following boundary conditions, see [AMPB08; TB93] for example,

$$\begin{aligned} u(0) &= v_0^\star \qquad u''(0) = 0 \\ u(L) &= v_L^\star \qquad u''(L) = 0 \end{aligned} \qquad (\textit{ad hoc} \text{ boundary conditions}). \tag{3.5}$$

In (3.5), the kinematic boundary conditions imposed at the start of the variational procedure have been supplemented with the 'natural' boundary conditions $u''(0) = 0$ and $u''(L) = 0$.

We will refer to these as *ad hoc* boundary conditions. The above energy reasoning that supports them has two flaws:

- The energy functional (3.4) is not positive-definite when $B<0$, making it unsuitable in a first place.
- Many other functionals differing from (3.4) by boundary terms equally deliver the stationarity condition (3.1) in the interior. There is no reason to believe that the boundary terms (3.5) delivered by the particular functional (3.4) are correct.

The *ad hoc* boundary conditions (3.5) are not accurate to order ε^2 and this lack of accuracy propagates to the solution to the boundary-value problem. This limitation in accuracy is already well known, but these ad hoc boundary conditions have a more harmful property: they create spurious oscillations in the solution $u_\varepsilon(x)$ when $B<0$. This can be seen from the general solution to the differential equation (3.1), which takes the following form when $B<0$,

$$u_\varepsilon(x) = D_1 \sin\Big(\frac{\omega x}{\varepsilon}\Big) + D_2 \cos\Big(\frac{\omega x}{\varepsilon}\Big) + D_3 x + D_4 - \frac{1}{K}\bar{f}^{(-2)}(x) - \frac{B}{K^2}\varepsilon^2 \bar{f}(x) + \mathcal{O}(\varepsilon^3), \tag{3.6}$$

where $\omega = \sqrt{K/(-B)}$ and $\bar{f}^{(-2)}$ is the second anti-derivative of the loading, such that $\bar{f}^{(-2)\prime\prime} = \bar{f}$. The constants D_1, D_2, D_3, D_4 are set by the boundary conditions: in Appendix A.2 we show that the *ad hoc* boundary conditions (3.5) make the amplitudes D_1 and D_2 associated with the quickly oscillating terms *non-zero* at the order ε^2 which we resolve. With $(D_1, D_2) = \mathcal{O}(\varepsilon^2)$ and $(D_3, D_4) = \mathcal{O}(\varepsilon^0)$, the fourth derivative u_ε'''' is dominated by the oscillatory terms, $u_\varepsilon'''' = \mathcal{O}(\varepsilon^{-2})$, making the gradient 'correction' $\varepsilon^2 B\, u_\varepsilon''''(x) = \mathcal{O}(\varepsilon^0)$ as large as the 'leading-order' term $K u_\varepsilon''(x) = \mathcal{O}(\varepsilon^0)$ in Equation (3.1). The short-wavelengths oscillations are fundamentally inconsistent with the main assumption underpinning homogenization, which is that $u_\varepsilon(x)$ is a function of the slow variable x having *regular* dependence on the aspect-ratio parameter ε, see the series expansion (4.2) below.

These short-wavelength oscillations are a long-standing issue that has hindered the use of strain-gradient models, most of which feature a non-positive strain-gradient stiffness B. The root of the issue is that the 'natural' boundary conditions $u''(0)=0$ and $u''(L)=0$ are incompatible with the leading order of the equilibrium (3.1) in the interior, which requires $u_\varepsilon''(0) = -\bar{f}(0)/K \neq 0$ and $u_\varepsilon''(L) = -\bar{f}(L)/K \neq 0$ (we ignore the special case $\bar{f}(0) = \bar{f}(L) = 0$ where the incompatibility is likely to be postponed at the following orders and not entirely suppressed). This incompatibility between the leading order and the boundary conditions makes the oscillatory 'correction' proportional to D_1 and D_2 blow up, and it ends up contributing as much as the leading-order term to the equilibrium equation.

We argue that these issues are artifacts introduced by the *ad hoc* boundary conditions, which go away when the mathematically rigorous boundary conditions are used. Indeed, it is shown in Appendix A.1 that the rigorous boundary conditions lead to $D_1 = D_2 = 0$ at the order ε^2 which we are resolving. The gradient effect then remains a small correction, and it becomes possible to solve the boundary-value problem perturbatively, as we show in Section 7.

Remark 3.2. The homogenized equilibrium (3.1) with the 'wrong' sign $B<0$ is akin to the so-called *bad Boussinesq equation* derived by Boussinesq to model the dynamics of shallow-water waves [Bou72]. The latter has a wide range of applications in physics and was historically used, in particular, to describe the propagation of non-linear wave in lattices, referred as the Fermi–Pasta–Ulam (FPU) problem [KZ64].

Remark 3.3. In a dynamic context again, and limiting attention to a simple chain of springs (with closest-neighbor interactions only), [KP09] obtained 'short-wave extraneous solutions' similar to the quickly oscillatory solutions associated with D_1 and D_2 in (3.6). They interpret the latter as 'artefacts left after the truncation of an infinite series'. Postulating that these extraneous solutions must disappear, they introduce boundary conditions which, in the low-frequency limit $\omega \to 0$, take the form $u''(x) = -\bar{f}(x)/K$ at $x=0$ and $x=L$. This is precisely the form of the boundary conditions which we will derive based on the analysis of the boundary layers, see Equation (3.7) and Section 5 .

3.3. Matched-asymptotic expansions to the rescue

The matched-asymptotic expansion technique [BO99; Eck73; Ili92; Lag88] is suited to mathematical problems whose solutions feature qualitatively different behaviors in different parts of the domain. It consists in analyzing the different regions using different types of approximations, and matching them together in a region of overlap where they are consistent. It is well suited to the analysis of the one-dimensional lattice in the limit $\varepsilon \to 0$ of well-separated scales:

- In the so-called *outer* region ($x \gg \varepsilon$ and $L - x \gg \varepsilon$, yellow background in Figure 3.1), the solution evolves 'slowly': the displacement in one cell closely resembles that in the neighboring cells.
- In the so-called *inner* regions ($x \ll L$ or $L - x \ll L$, blue background in Figure 3.1), the solution evolves rapidly from one cell to the next.

The traditional names of *outer* and *inner* regions from matched-asymptotic theory are unfortunately in conflict with their actual layout in this particular geometry: the outer region is the central part of the lattice (yellow) and the inner regions are near the endpoints (blue).

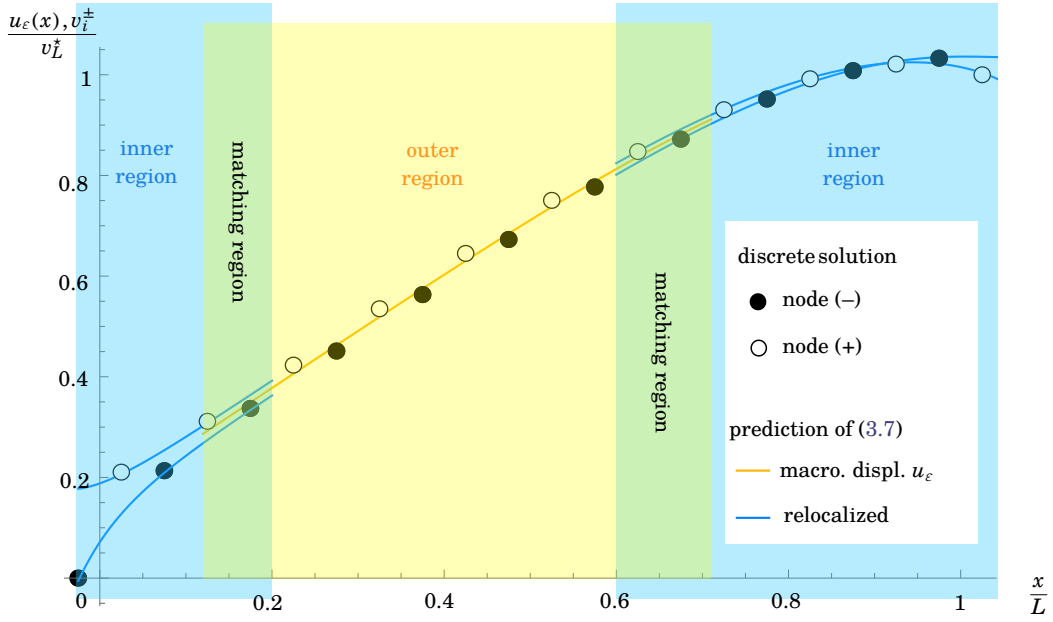

Figure 3.1. Numerical solution to the discrete problem with $N = 10$, (*i.e.*, 11 cells and 22 nodes) (solid and open disks). Qualitatively different behaviors are obtained in the inner regions (blue background) and in the outer region (yellow background), which motivates the use of matched asymptotic expansion. The predictions of the latter are shown by the solid curves (see Figure 3.2 for details).

In the outer region, the homogenization theory applies: the displacement of the nodes belonging to either type of sub-lattice, + or –, varies smoothly and can thus be considered to be a function of the *slow* variable x. The two sub-lattices are however shifted with respect to one another, and the displacement of the full set of nodes has an oscillatory component known as the *microscopic shift*: the open and solid disks are alternated across the brown midline in the outer region in Figure 3.1. The macroscopic displacement $u_\varepsilon(x)$ is defined as the *averaged* displacement over the two Bravais sub-lattices (brown curve in the figure). The averaging removes the oscillatory microscopic shift and $u_\varepsilon(x)$ is a smooth function of x, evolving on the large scale $\mathcal{O}(\varepsilon^0)$. This is implemented in a systematic expansion in Section 4, which delivers the differential equation (3.1) of homogenized equilibrium.

By contrast, the analysis of the boundary layers involves zooming in at the microscopic scale ε, by setting $x = \varepsilon i$ with moderately large values of $i = \mathcal{O}(\varepsilon^{-1/2})$ (case of endpoint on the left-hand side): at this scale, the loading can be approximated by its Taylor expansion $\bar{f}(\varepsilon i) = \bar{f}(0) + \varepsilon i \bar{f}'(0) + \cdots$, which is polynomial, and the geometry of the domain is effectively semi-infinite. The analysis of a boundary layer consists in deriving an exact solution to the discrete equilibrium problem, which has constant coefficients in the interior and a polynomial right-hand side (applied loading). These layer problems are solved in Section 5 in terms of four constants.

In Section 6, we proceed to match the inner and outer solutions: in the matching region $\varepsilon \ll x \ll L$ (case of the left-hand side, green region in Figure 3.1), for instance, both the inner solution ($x \ll L$) and the outer solution ($\varepsilon \ll L$) are valid. By requiring that they are consistent, we can determine the four constants characterizing the inner region in terms of the local properties of the outer solution, namely $u_\varepsilon(0)$, $u_\varepsilon'(0)$, $u_\varepsilon''(0)$, etc. The same holds in the other matching region. When the parameters of the inner regions are eliminated, the procedure delivers effective boundary conditions applicable at either end $x = 0$ and $x = L$ of the macroscopic domain. This yields the rigorous boundary conditions appearing in Equation (3.7) below. The entire procedure is a systematic expansion in ε, and we ensure that the order of accuracy of the boundary conditions is consistent with the second-order accuracy which we achieve in the outer region.

Altogether, this leads to the following boundary-value problem,

$$\begin{aligned} &\text{diff. equation} && K u''(x) - \varepsilon^2 B u^{(4)}(x) + \bar{f}(x) = 0 \\ &\text{boundary cond.} && \begin{cases} u(0) + \varepsilon\, \ell_0 u'(0) + \varepsilon^2 \tilde{\ell}_0 u''(0) &= v_0^\star \\ \varepsilon^2 \left(K u''(0) + \bar{f}(0)\right) &= 0 \\ u(L) + \varepsilon\, \ell_L u'(L) + \varepsilon^2 \tilde{\ell}_L u''(L) &= v_L^\star \\ \varepsilon^2 \left(K u''(L) + \bar{f}(L)\right) &= 0, \end{cases} \end{aligned} \tag{3.7}$$

where the differential equation coincides with that announced earlier in (3.1). This boundary-value problem is the main result of our paper. Its solution $u(x)$ depends on x and is denoted as $u_\varepsilon(x)$ in the following.

At the endpoint $x=0$, the first, Robin-type boundary condition $u(0)+\varepsilon\,\ell_0\,u'(0)+\varepsilon^2\,\tilde{\ell}_0\,u''(0)=v_0^\star$ is a *refined* version of the naïve kinematic condition $u(0)=v_0^\star$ postulated in (3.5). Indeed, the fixed-displacement condition $v_0^-=v_0^\star$ in $(2.4)_1$ concerns the first node, of type (–), whose position is given by the *macroscopic* displacement $u(0)$ at leading order *plus corrections* of order ε. The microscopic lengths $\varepsilon\,\ell_0$ and $\varepsilon^2\,\tilde{\ell}_0$ entering in the corrected boundary condition are furnished by the boundary layer analysis, see Equations $(5.11)_{3,4}$.

The second boundary condition at $x=0$, namely $\varepsilon^2\,(K\,u''(0)+\bar{f}(0))=0$, is a *corrected* version of the naïve boundary condition $u''(0)=0$ obtained in (3.5). This correction removes the inconsistencies discussed in Section 3.2. We will refer to it as a *compatibility condition*.

The boundary conditions at $x=L$ are exactly similar, with the constants ℓ_L and $\tilde{\ell}_L$ given in (6.11).

In equation (3.7), we have included an overall scaling factor ε^2 in the boundary conditions $\varepsilon^2\,(K\,u''(x_i)+\bar{f}(x_i))=0$ at $x_i=0,L$ to indicate that only the leading order term of this boundary condition is known, *i.e.*, $\varepsilon^2\,(K\,u''(x_i)+\bar{f}(x_i))=\mathcal{O}(\varepsilon^3)$. This writing complies with the convention used throughout this paper that all equations are truncated beyond order ε^2. When written as $K\,u''(x_i)+\bar{f}(x_i)=0$, the boundary condition could be interpreted as $K\,u''(x_i)+\bar{f}(x_i)=\mathcal{O}(\varepsilon^3)$, which is not correct.

3.4. Comparison to the discrete solution

Figures 3.1 and 3.2 show a first comparison of the solution $u_\varepsilon(x)$ to the boundary-value problem (3.7) with the discrete solution to the lattice problem (2.8), for a particular loading. In Section 8, more elaborate convergence tests are used to show that the boundary-value problem (3.7) is accurate up to terms of order ε^3.

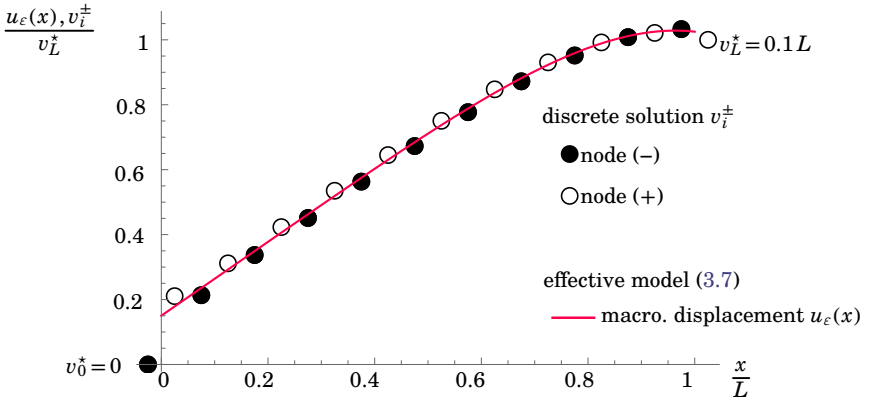

Figure 3.2. Comparison of the macroscopic displacement $u_\varepsilon(x)$ solution to the boundary-value problem (3.7) (red curve) with the discrete solution for $N=10$ (solid and open disks), for a distributed loading $\bar{f}(x)=2\,k_1/L\,(x/L)^3$ and with imposed displacements $v_0^\star=0$ and $v_L^\star=0.1\,L$ at the endpoints. The spring constants listed in Table 2.1 are used. The displacements on the vertical axis have been rescaled by $v_L^\star$.

4. HOMOGENIZATION

In this Section we derive an effective model for the lattice in the outer region ($\varepsilon\ll x$ and $L-x\gg\varepsilon$, yellow box in Figure 4.1) using asymptotic homogenization. This procedure is standard and the details are omitted.

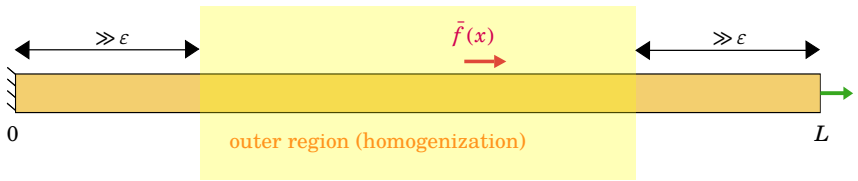

Figure 4.1. Far from the endpoints (outer region, yellow box), the equilibrium is solved using asymptotic homogenization.

4.1. Form of the expansion

In the outer region, the displacement $v_i^\pm$ of the node $(i,\pm)$ is assumed to derive from smooth functions $u_\varepsilon(x)$ and $y_\varepsilon(x)$ of the slow variable x, representing the *macroscopic displacement* and the *microscopic shift* (see Section 3.3), respectively,

$$v_i^\pm=u_\varepsilon(x_i^\pm)\pm\varepsilon\,y_\varepsilon(x_i^\pm),\tag{4.1}$$

where $x_i^{\pm}$ is the position of the node in reference configuration, see (2.1). Making u_ε and y_ε depend on the slow variable ensures that they vary by a small amount $\sim u'_\varepsilon(x)\varepsilon = \mathcal{O}(\varepsilon)$ and $\sim y'_\varepsilon(x)\varepsilon = \mathcal{O}(\varepsilon)$, respectively, from one cell to the next.

We approach homogenization through *formal* asymptotic expansions: we thus assume that $u_\varepsilon(x)$ and $y_\varepsilon(x)$ depend on ε through *regular* (power-series) expansions,

$$u_\varepsilon(x) = \sum_{i=0}^{\infty} \varepsilon^i u_{(i)}(x), \qquad y_\varepsilon(x) = \sum_{i=0}^{\infty} \varepsilon^i y_{(i)}(x), \tag{4.2}$$

where the series coefficients $u_{(i)}(x)$ and $y_{(i)}(x)$ are themselves smooth functions of x that do not depend on ε. We will avoid as much as possible to expose the series expansion (4.2) as they lead to cumbersome expressions. The main concrete consequence of the existence of the regular expansions (4.2) is that the derivatives remain of the same order as the functions: we will systematically assume

$$u_\varepsilon(x) = \mathcal{O}(\varepsilon^0), \quad u'_\varepsilon(x) = \mathcal{O}(\varepsilon^0), \quad u''_\varepsilon(x) = \mathcal{O}(\varepsilon^0), \quad \dots \quad y_\varepsilon(x) = \mathcal{O}(\varepsilon^0), \quad y'_\varepsilon(x) = \mathcal{O}(\varepsilon^0), \quad \dots \tag{4.3}$$

Remark 4.1. In the right-hand side of (4.1), both $u_\varepsilon(x)$ and $y_\varepsilon(\varepsilon)$ are $\mathcal{O}(\eta^0)$, as the following order-of-magnitude reasoning suggests. Anticipating that the homogenized equilibrium takes the standard form $u''_\varepsilon \sim \bar{f}$ at leading order with $\bar{f} = \mathcal{O}(\varepsilon^0)$ as the distributed load, we obtain the following estimates: $u_\varepsilon(x) = \mathcal{O}(\varepsilon^0)$ for the displacement, $u'_\varepsilon(x) = \mathcal{O}(\varepsilon^0)$ for the strain, $\varepsilon u'_\varepsilon(x) = \mathcal{O}(\varepsilon^1)$ for the changes in spring length. This is exactly what (4.1) was designed for: for short springs of type 1, for instance, the change in spring length is $v_i^+ - v_i^- \approx u'_\varepsilon(\varepsilon i)\ (\varepsilon/2) + 2\varepsilon y_\varepsilon(\varepsilon i)$, both the contributions $\varepsilon u'_\varepsilon/2 = \mathcal{O}(\varepsilon)$ and $2\varepsilon y_\varepsilon = \mathcal{O}(\varepsilon)$ being of order ε.

In the interior of the lattice (traditionally and unfortunately called the 'outer' region), the displacement vector $\boldsymbol{V}_i = (\ v_i^-\ \ v_i^+\ )$ introduced in (2.5) can be written using (4.1) and (2.1–2.2) as $\boldsymbol{V}_i = \boldsymbol{V}_i^{\text{int}}$ where

$$\begin{aligned} \boldsymbol{V}_i^{\text{int}} &= \begin{pmatrix} u(x_i^-) - \varepsilon y(x_i^-) \\ u(x_i^+) + \varepsilon y(x_i^+) \end{pmatrix} \\ &= \begin{pmatrix} u(x_i - \delta) - \varepsilon y(x_i - \delta) \\ u(x_i + \delta) + \varepsilon y(x_i + \delta) \end{pmatrix} \\ &= \left[\begin{pmatrix} u - \varepsilon y \\ u + \varepsilon y \end{pmatrix} + \varepsilon\,\delta \begin{pmatrix} -u' + \varepsilon y' \\ u' + \varepsilon y' \end{pmatrix} + \frac{\varepsilon^2\,\delta^2}{2} \begin{pmatrix} u'' - \varepsilon y'' \\ u'' + \varepsilon y'' \end{pmatrix} + \cdots \right]_{x=\varepsilon i}. \end{aligned} \tag{4.4}$$

In the interest of legibility we have dropped the subscripts in both u_ε and y_ε in the above equation.

In the last equality in (4.4), we have Taylor-expanded the functions u_ε, y_ε and their derivatives about the cell center εi. We recall that $\delta = 1/4$ by (2.2).

4.2. Homogenized equilibrium equations

The homogenized equations of equilibrium are obtained by inserting the expansion of the displacement (4.4) into the discrete-difference equation $(2.8)_1$ governing the equilibrium of a node i in the outer region (for $1 \ll i$ and $N - i \gg 1$). In this equilibrium equation, the shifted terms $\boldsymbol{P}\cdot\boldsymbol{V}_{i+1}^{\text{int}}$ and $\boldsymbol{R}\cdot\boldsymbol{V}_{i-1}^{\text{int}}$ are given by (4.4) as series expansions about $x = \varepsilon\,(i+1)$ and $x = \varepsilon\,(i-1)$, respectively, and another Taylor expansion is needed to rewrite each of them as an expansion about the common cell center $x = \varepsilon i$. The force term $\boldsymbol{F}_i = \frac{\varepsilon}{2}\bar{\boldsymbol{F}}_\varepsilon(\varepsilon i) = \frac{\varepsilon}{2}\left(\ \bar{f}(\varepsilon\,(i-\delta))\ \ \bar{f}(\varepsilon\,(i+\delta))\ \right)$, see (2.7) and (2.11), is expanded about $x = \varepsilon i$ as well. This yields the expansion of the equilibrium $(2.8)_1$ given in Equation (B.1) in Appendix B.

At this point, there are two options:

- The standard approach is to insert the series expansions (4.2) of u_ε and y_ε and read off Equation (B.1) order by order. This yields a hierarchy of equations relating the series coefficients $u_{(k)}(x)$ and $y_{(k)}(x)$. These equations are then solved, yielding (*i*) expressions for the $y_{(k)}$'s in terms of the $u_{(k)}$'s and their derivatives, and (*ii*) compatibility conditions for the $u_{(k)}$'s and their derivatives. As a last step, these expressions are 're-summed' so as to restore the original quantities $u_\varepsilon(x)$ and $y_\varepsilon(x)$: the family of equations (*i*) yields the microscopic shift $y_\varepsilon(x)$ in terms of the macroscopic strain $u'_\varepsilon(x)$ and its derivatives, while the family (*ii*) yields the homogenized equilibrium. The drawback of this approach is that the intermediate steps involve cumbersome and highly redundant expressions.

- We propose a more concise derivation, which starts from the anticipated form of the final result, namely (*i*) that the microscopic shift $y_\varepsilon(x)$ is a linear combination of the strain $u'_\varepsilon(x)$ and to its successive derivatives,

  $$y_\varepsilon(x) = \varepsilon^0 Y_0 u'_\varepsilon(x) + \varepsilon^1 Y_1 u''_\varepsilon(x) + \varepsilon^2 Y_2 u'''_\varepsilon(x) + \mathcal{O}(\varepsilon^3), \tag{4.5}$$

  and (*ii*) that the homogenized equilibrium is of the form

  $$\bar{f}(x) + A_0 u''_\varepsilon(x) + \varepsilon A_1 u'''_\varepsilon(x) + \varepsilon^2 A_2 u^{(4)}_\varepsilon(x) + \cdots = 0. \tag{4.6}$$

  The coefficients $(Y_i)_{i\geqslant 0}$ and $(A_i)_{i\geqslant 0}$ are identified by inserting these expressions into the Taylor expansion (B.1) of the equilibrium in interior nodes ($0 < i < N$), using the series expansions (4.2).

The second approach is implemented in the companion notebook. The result is

$$Y_0=\frac{1}{8},\qquad Y_1=\frac{1}{16},\qquad Y_2=\frac{1}{48},\quad \dots \tag{4.7}$$

and

$$A_0=\frac{15k_1}{4},\qquad A_1=0,\qquad A_2=\frac{9k_1}{32},\qquad \dots$$

With $A_1=0$, the equilibrium (4.6) matches the form anticipated in (3.1) up to terms of order ε^3: the elastic moduli are identified as $K=A_0$ and $B=-A_2$ in agreement with the values announced in (3.2).

Equations (4.5) and (4.7) yield the microscopic shift $y_\varepsilon(x)$ in terms of the strain $u'_\varepsilon(x)$ and its gradients, which is the main task of homogenization. Inserting this into (4.1) yields the nodal displacement $v_i^\pm$ in terms of the macroscopic displacement $u_\varepsilon(x)$. Equivalently, we can insert (4.5) into (4.4) and obtain the relocalization formula for the nodal positions $\boldsymbol{V}_i=(v_i^-,v_i^+)$ as

$$\boldsymbol{V}_i^{\text{int}}=u_\varepsilon(\varepsilon i)\,\boldsymbol{W}_0+\varepsilon u'_\varepsilon(\varepsilon i)\,\boldsymbol{W}_1+\varepsilon^2 u''_\varepsilon(\varepsilon i)\,\boldsymbol{W}_2+\mathcal{O}(\varepsilon^3), \tag{4.8}$$

where

$$\begin{aligned}\boldsymbol{W}_0 &= \begin{pmatrix}1\\1\end{pmatrix}\\ \boldsymbol{W}_1 &= \left(Y_0+\frac{1}{4}\right)\begin{pmatrix}-1\\1\end{pmatrix} = \frac{3}{8}\begin{pmatrix}-1\\1\end{pmatrix}\\ \boldsymbol{W}_2 &= \frac{1+8Y_0}{32}\begin{pmatrix}1\\1\end{pmatrix}+Y_1\begin{pmatrix}-1\\1\end{pmatrix} = \frac{1}{8}\begin{pmatrix}0\\1\end{pmatrix}.\end{aligned} \tag{4.9}$$

In Equation (4.8), the successive terms in the right-hand side represent (*i*) the macroscopic displacement, (*ii*) the leading-order contribution to the microscopic shift, proportional to the local strain value $u'_\varepsilon(\varepsilon i)$, and (*ii*) the next-order correction to the microscopic shift, proportional to the strain gradient $u''_\varepsilon(\varepsilon i)$.

5. BOUNDARY LAYER ANALYSIS

We proceed to analyze the layers forming near the endpoints $i=0$ and $i=N$. Ignoring the exponentially small coupling between these two layers and focussing on the endpoint $i=0$, we assume that the lattice is *semi-infinite* ($i\geqslant 0$), see Figure 5.1. The boundary layer analysis is concerned with a small region near the endpoint $i=0$, namely $i\ll N=\mathcal{O}(\varepsilon^{-1})$, corresponding to a small part of the full lattice, $x\ll L$. Specifically, we will limit attention to *moderately large* index values i,

$$i=\mathcal{O}(\varepsilon^{-1/2}). \tag{5.1}$$

We could equally pick any power q in the range $-1<q<0$ as we will only use $1\ll i\ll\varepsilon^{-1}$.

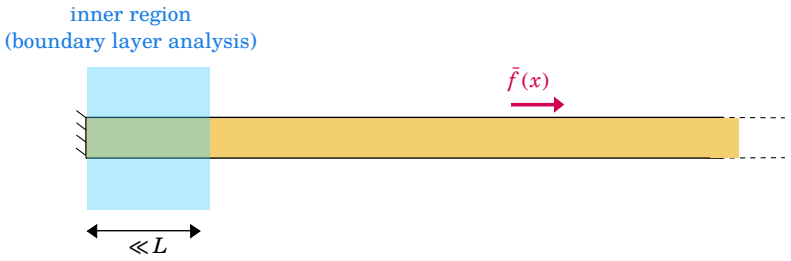

Figure 5.1. A boundary layer analysis is undertaken in the inner region, of size $\ll L$ near the boundary $x=0$ (blue region). The boundary layer 'sees' the bar as semi-infinite.

The boundary layer near the other endpoint $x=L$ can be obtained without any further calculation by applying the mirror-symmetry $i\longrightarrow N-i$ to the results obtained for the endpoint $x=0$.

5.1. Boundary-layer modes

The first step of the boundary-layer analysis is to work out the general solution to the discrete-difference equation $(2.8)_1$ governing the equilibrium in interior cells ($0<i<N$). We start in this section with the special case of a zero applied force ($\boldsymbol{F}_i=\boldsymbol{0}$).

For $\boldsymbol{F}_i=\boldsymbol{0}$ and $i>0$, we seek solutions to $(2.8)_1$ in the form

$$\boldsymbol{V}_i=\mu^{-i}\boldsymbol{U}(i) \tag{5.2}$$

where μ is *a priori* a complex number and $\boldsymbol{U}(i)$ is a vector having *polynomial* dependence on i. This leads to the following generalized eigenvalue problem

$$\mu^{-2}\boldsymbol{P}\cdot\boldsymbol{U}(i+1)+\mu^{-1}\boldsymbol{Q}\cdot\boldsymbol{U}(i)+\boldsymbol{R}\cdot\boldsymbol{U}(i-1)=\boldsymbol{0}, \tag{5.3}$$

in which the unknowns are both the polynomial $\boldsymbol{U}(i)$ (generalized eigenvector) and the complex number μ (eigenvalue).

Using symbolic calculations, we obtain four pairs of solutions $(\mu_p, \boldsymbol{U}_p(i))_{p=1,\dots,4}$ of (5.3) in the form

p	1	2	3	4
μ_p	ζ^{+1}	ζ^{-1}	1	1
$\boldsymbol{U}_p(i)$	$\boldsymbol{\Lambda}_0$	$\tilde{\boldsymbol{\Lambda}}_0$	$\boldsymbol{W}_1 + \boldsymbol{W}_0 i$	$\boldsymbol{W}_0$

(5.4)

where all eigenvalues μ_p turn out to be real, and we denote by $\zeta = \mu_1 > 1$ the largest one. For the special values of the elastic contrasts listed in Table 2.1, the constants entering in the exponential modes are

$$\begin{aligned} \zeta &\approx 9.39 \\ \boldsymbol{\Lambda}_0 &\approx \begin{pmatrix} -8.34 & 1 \end{pmatrix} \\ \tilde{\boldsymbol{\Lambda}}_0 &\approx \begin{pmatrix} -0.377 & 1 \end{pmatrix}. \end{aligned} \tag{5.5}$$

In the companion notebook, these constants are expressed more generally in terms of the spring contrasts $(k_2/k_1, \dots, k_4/k_1)$.

In (5.4), the eigenvalue $\mu_3 = \mu_4 = 1$ is double, which is why the eigenvector $\boldsymbol{U}(i)$ had to be sought in the form of a polynomial and not just a constant. These modes represent uniform stretching ($p = 3$) and a rigid-body translation ($p = 4$)—note that they use the same $\boldsymbol{W}_i$'s as in (4.8–4.9). They match the macroscopic solutions $u_\varepsilon(x) = x$ and $u_\varepsilon(x) = 1$ in the homogenized solution (4.8–4.9), respectively.

To sum up, the general *homogeneous* solution to Equation $(2.8)_1$ governing the equilibrium in interior cells ($i > 0$) takes the form

$$\boldsymbol{V}_i^{\mathrm{h}} = C_1\, \zeta^{-i}\, \boldsymbol{\Lambda}_0 + C_2\, \zeta^{+i}\, \tilde{\boldsymbol{\Lambda}}_0 + C_3\, (\boldsymbol{W}_1 + \boldsymbol{W}_0 i) + C_4 \begin{pmatrix} 1 \\ 1 \end{pmatrix}. \tag{5.6}$$

where $\begin{pmatrix} C_1 & \cdots & C_4 \end{pmatrix}$ are four free parameters.

5.2. Boundary-layer solution

We proceed to find the general solution in the boundary layer.

1. We start by identifying a *particular* solution to the equilibrium $(2.8)_1$ in the interior cells ($i > 0$), taking the nodal force $\boldsymbol{F}_i = \frac{\varepsilon}{2} \bar{\boldsymbol{F}}_\varepsilon(\varepsilon i)$ into account, see (2.11). To this end, we observe that the equilibrium $(2.8)_1$ in the interior cells of the boundary layer ($i > 0$) is identical to the equilibrium $(2.8)_1$ in the outer region, which we addressed during homogenization in Section 4. Particular solutions to Equation $(2.8)_1$ in the boundary layer can therefore be generated easily, by inserting any particular function $u_{\mathrm{p}}(x)$ satisfying the homogenized equilibrium (3.1) into the relocalization formula (4.8). We choose the generating function

$$u_{\mathrm{p}}(x) = -\left(\frac{\bar{f}(0)}{2K} x^2 + \frac{\bar{f}'(0)}{6K} x^3 + \frac{\bar{f}''(0)}{K} \left(\frac{x^4}{24} + \varepsilon^2 \frac{B x^2}{2K} \right) \right) + \mathcal{O}\left(\max\left(x^5, \varepsilon^2 x^3, \varepsilon^3\right)\right), \tag{5.7}$$

   which was obtained by solving the homogenized equilibrium (3.1) order by order with respect to both $\varepsilon \ll 1$ and $x \ll 1$, with arbitrary initial conditions $u_{\mathrm{p}}(0) = u_{\mathrm{p}}'(0) = 0$. The remainder in the right-side of (5.7) lists the various kinds of terms that we have neglected in the expansion. In view of (4.8) the nodal displacement is given by $\boldsymbol{V}_i^{\mathrm{p}} = u_{\mathrm{p}}(\varepsilon i)\, \boldsymbol{W}_0 + \varepsilon u_{\mathrm{p}}'(\varepsilon i)\, \boldsymbol{W}_1 + \varepsilon^2 u_{\mathrm{p}}''(\varepsilon i)\, \boldsymbol{W}_2 + \mathcal{O}(\varepsilon^3)$. Inserting (5.7), truncating the right-hand side to order ε^2 included, and using the scaling assumption $i = \mathcal{O}(\varepsilon^{-1/2})$ in (5.1), we get a particular solution in the boundary layer in the form

$$\boldsymbol{V}_i^{\mathrm{p}} = -\frac{1}{K} \left[\begin{array}{l} \left(\dfrac{\bar{f}(0)}{2} \varepsilon^2 i^2 + \dfrac{\bar{f}'(0)}{6} \varepsilon^3 i^3 + \dfrac{\bar{f}''(0)}{24} \varepsilon^4 i^4 \right) \boldsymbol{W}_0 \\ + \varepsilon \left(\bar{f}(0)\, \varepsilon i + \dfrac{\bar{f}'(0)}{2} \varepsilon^2 i^2 \right) \boldsymbol{W}_1 + \varepsilon^2 \bar{f}(0)\, \boldsymbol{W}_2 \end{array} \right] + \mathcal{O}(\varepsilon^{5/2}). \tag{5.8}$$

   It can be checked directly that this is a solution to the equilibrium $(2.8)_1$ in the interior cells ($i > 0$). Unlike generic solutions, this particular solution is free of exponential terms by construction.

2. Next, we combine this particular solution with the general homogeneous solution (5.6). This yields the generic solution to Equation $(2.8)_1$ governing the equilibrium of interior nodes ($i > 0$) as

$$\begin{aligned} \boldsymbol{V}_i^{\mathrm{BL}} \;=\; & C_1\, \zeta^{-i}\, \boldsymbol{\Lambda}_0 + C_2\, \zeta^{+i}\, \tilde{\boldsymbol{\Lambda}}_0 \\ & + \left\{ C_4 + i C_3 - \frac{1}{K} \left(\frac{\bar{f}(0)}{2} \varepsilon^2 i^2 + \frac{\bar{f}'(0)}{6} \varepsilon^3 i^3 + \frac{\bar{f}''(0)}{24} \varepsilon^4 i^4 \right) \right\} \boldsymbol{W}_0 \\ & + \left\{ C_3 - \frac{\varepsilon}{K} \left(\bar{f}(0)\, \varepsilon i + \frac{\bar{f}'(0)}{2} \varepsilon^2 i^2 \right) \right\} \boldsymbol{W}_1 + \varepsilon^2 \left\{ -\frac{\bar{f}(0)}{K} \right\} \boldsymbol{W}_2 + \mathcal{O}(\varepsilon^{5/2}). \end{aligned} \tag{5.9}$$

3. The last step is to take the equilibrium of the first cell $i = 0$ into account. The applied load is given by (2.7), (2.11) and (2.12) as

$$\boldsymbol{F}_0 = \frac{\varepsilon}{2} \bar{\boldsymbol{F}}_\varepsilon(0) + \boldsymbol{\Delta}_0 = \begin{pmatrix} -\frac{v_0^\star}{\varepsilon} \\ \frac{\varepsilon}{2} \bar{f}(\varepsilon \delta) \end{pmatrix} = -\frac{v_0^\star}{\varepsilon} \begin{pmatrix} 1 \\ 0 \end{pmatrix} + \frac{\varepsilon}{2} \bar{f}(0) \begin{pmatrix} 0 \\ 1 \end{pmatrix} + \mathcal{O}(\varepsilon^2).$$

Inserting (5.9) into $(2.8)_2$, we get two linear equations which we solve for C_1 and C_4 as

$$\begin{pmatrix} C_1 \\ C_4 \end{pmatrix} = \begin{pmatrix} * & \rho_0 & \chi_0/K & 0 \\ * & -\ell_0 & \tilde{\ell}_0/K & 1 \end{pmatrix} \cdot \begin{pmatrix} C_2 \\ C_3 \\ \varepsilon^2 \bar{f}(0) \\ v_0^\star \end{pmatrix} + \mathcal{O}(\varepsilon^{5/2}), \tag{5.10}$$

where the symbols $*$ in the matrix denote numeric constants which we do not need to determine. With the stiffness ratios listed in Table 2.1, the other constants are given by

$$\begin{aligned} \rho_0 &\approx 0.119 \\ \chi_0 &\approx 0.0149 \\ \ell_0 &\approx -1.37 \\ \tilde{\ell}_0 &\approx 0.124. \end{aligned} \tag{5.11}$$

The expressions of $(\rho_0, \chi_0, \ell_0, \tilde{\ell}_0)$ for arbitrary stiffness ratios $(k_0/k_1, k_2/k_1, \dots, k_4/k_1)$ are worked out in the companion notebook [Thb24].

The boundary-layer solution is given by (5.9–5.10) in terms of the applied loading $\bar{f}(0)$, of the imposed displacement $v_0^\star$, and of two constants C_2 and C_3 which are determined in the next section.

6. MATCHING

In this Section, we proceed to match the outer solution from Section 4 with the inner solution from Section 5, following the standard procedure of matched asymptotic expansions [BO99; Eck73; Ili92; Lag88]. The matching procedure delivers two effective boundary conditions on the macroscopic field $u_\varepsilon(x)$ and its derivatives at each of the endpoints. The matching takes place in the region $\varepsilon \ll x \ll L$ near the endpoint $x = 0$ on the one hand, and in the region $\varepsilon \ll L - x \ll L$ near the endpoint $x = L$ on the other hand. In each of these regions, both the outer solution $\boldsymbol{V}_i^{\text{int}}$ for the nodal displacement and the inner solution $\boldsymbol{V}_i^{\text{BL}}$ are valid and we require that they coincide to the order which we resolve.

The matching conditions about $x = 0$ are derived in Section 6.1. The matching conditions at the endpoint $x = L$ are deduced in Section 6.2 without any further calculation, by applying a mirror symmetry.

6.1. Matching about first endpoint, $x = 0$

The matching region near the endpoint $x = 0$ is the overlap of the regions of validity of the outer and inner solutions, namely

$$1 \ll i \quad \text{and} \quad i = O(\varepsilon^{-1/2}). \tag{6.1}$$

The outer solution $\boldsymbol{V}_i^{\text{int}}$ in (4.8) can be expanded for $\varepsilon i = \mathcal{O}(\varepsilon^{1/2}) \ll 1$ as

$$\boldsymbol{V}^{\text{int}}(\varepsilon i) = \begin{Bmatrix} & i^0 & (& u_\varepsilon(0)\,\boldsymbol{W}_0 & + & \varepsilon u_\varepsilon'(0)\,\boldsymbol{W}_1 & + & \varepsilon^2 u_\varepsilon''(0)\,\boldsymbol{W}_2 &) \\ + & i^1 & (& \varepsilon u_\varepsilon'(0)\,\boldsymbol{W}_0 & + & \varepsilon^2 u_\varepsilon''(0)\,\boldsymbol{W}_1 & & &) \\ + & i^2/2 & (& \varepsilon^2 u_\varepsilon''(0)\,\boldsymbol{W}_0 & + & \varepsilon^3 u_\varepsilon'''(0)\,\boldsymbol{W}_1 & & &) \\ + & i^3/6 & (& \varepsilon^3 u_\varepsilon'''(0)\,\boldsymbol{W}_0 & & & & &) \\ + & i^4/24 & (& \varepsilon^4 u_\varepsilon''''(0)\,\boldsymbol{W}_0 & & & & &) \end{Bmatrix} + \mathcal{O}(\varepsilon^{5/2}). \tag{6.2}$$

This polynomial function of i cannot be matched for all i's in the range (6.1) with the boundary-layer solution (5.9) unless the dominant, exponentially growing term proportional to C_2 vanishes in the latter. This yields a first matching condition

$$C_2 = 0 + \mathcal{O}(\varepsilon^{5/2}). \tag{6.3}$$

Inserting it in (5.10), we then get

$$\begin{pmatrix} C_1 \\ C_4 \end{pmatrix} = \begin{pmatrix} \rho_0 C_3 + \varepsilon^2 \frac{\chi_0}{K} \bar{f}(0) \\ v_0^\star - \ell_0 C_3 + \varepsilon^2 \frac{\tilde{\ell}_0}{K} \bar{f}(0) \end{pmatrix} + \mathcal{O}(\varepsilon^{5/2}), \tag{6.4}$$

and the boundary-layer solution in (5.9) becomes

$$\boldsymbol{V}_i^{\text{BL}} = \begin{Bmatrix} \zeta^{-i} & (& \rho_0 C_3\,\boldsymbol{\Lambda}_0 & + & \varepsilon^2 \frac{\chi_0}{K} \bar{f}(0)\,\boldsymbol{\Lambda}_0 & &) \\ + i^0 & (& (v_0^\star - \ell_0 C_3)\,\boldsymbol{W}_0 & + & C_3 \boldsymbol{W}_1 & + \frac{\varepsilon^2}{K}(\tilde{\ell}_0 \boldsymbol{W}_0 - \boldsymbol{W}_2)\,\bar{f}(0) &) \\ + i^1 & (& C_3 \boldsymbol{W}_0 & - & \varepsilon^2 \frac{\bar{f}(0)}{K} \boldsymbol{W}_1 & &) \\ + \frac{i^2}{2} & (& -\varepsilon^2 \frac{\bar{f}(0)}{K} \boldsymbol{W}_0 & - & \varepsilon^3 \frac{\bar{f}'(0)}{K} \boldsymbol{W}_1 & &) \\ + \frac{i^3}{6} & (& -\varepsilon^3 \frac{\bar{f}'(0)}{K} \boldsymbol{W}_0 & & & &) \\ + \frac{i^4}{24} & (& -\varepsilon^4 \frac{\bar{f}''(0)}{K} \boldsymbol{W}_0 & & & &) \end{Bmatrix} + \mathcal{O}(\varepsilon^{5/2}). \tag{6.5}$$

The matching procedure involves identifying the polynomial coefficients appearing in parentheses in (6.2) and (6.5): the term on the first line of (6.5) is exponentially small, and therefore negligible in the matching region, where $i \gg 1$. Processing the powers of i in decreasing order, we get the following matching conditions

$$\begin{array}{c|rcl|l} & \boldsymbol{W}_0 & & & \boldsymbol{W}_1 \\ \hline i^4 & \varepsilon^2(K u_\varepsilon''''(0) + \bar{f}''(0)) & = & \mathcal{O}(\varepsilon^{5/2}) & \\ i^3 & \varepsilon^{3/2}(K u_\varepsilon'''(0) + \bar{f}'(0)) & = & \mathcal{O}(\varepsilon^{5/2}) & \\ i^2 & \varepsilon^1(K u_\varepsilon''(0) + \bar{f}(0)) & = & \mathcal{O}(\varepsilon^{5/2}) & \text{(nothing new)} \\ i^1 & \varepsilon^{-1/2} C_3 & = & \varepsilon^{1/2} u_\varepsilon'(0) + \mathcal{O}(\varepsilon^{5/2}) & \text{(nothing new)} \\ i^0 & v_0^\star - \ell_0 C_3 & = & u_\varepsilon(0) + \varepsilon^2 \tilde{\ell}_0 (-\bar{f}(0)/K) + \mathcal{O}(\varepsilon^{5/2}) & \text{(nothing new)} \end{array} \tag{6.6}$$

We have used the fact that $\boldsymbol{W}_0$ and $\boldsymbol{W}_1$ are linearly independent to identify their respective coefficients separately, see the two columns in the table above. On the last line (constant coefficients), we have also used the fact that the two terms along $\boldsymbol{W}_2$ cancel out.

To sum up, we have obtained

- the expression of the last unknown coefficient in the boundary-layer solution (row i^1)

$$C_3 = \varepsilon u_\varepsilon'(0) + \mathcal{O}(\varepsilon^3), \tag{6.7}$$

- a compatibility condition (row i^2, multiplying by ε and truncating at order ε^3)

$$\varepsilon^2(K u_\varepsilon''(0) + \bar{f}(0)) = O(\varepsilon^3), \tag{6.8}$$

- a kinematic condition, obtained by inserting (6.7) into the matching condition labelled i^0 in the table, and eliminating $\bar{f}(0)$ using (6.8),

$$v_0^\star = u_\varepsilon(0) + \varepsilon \ell_0 u_\varepsilon'(0) + \varepsilon^2 \tilde{\ell}_0 u_\varepsilon''(0) + \mathcal{O}(\varepsilon^{5/2}). \tag{6.9}$$

Equation (6.8–6.9) are the asymptotic boundary conditions announced in (3.7). The constants ℓ_0 and $\tilde{\ell}_0$ have been determined by the boundary-layer analysis, see $(5.11)_{3,4}$.

Remark 6.1. We have proven in (6.9) that the boundary condition is exact to order ε^2 included and that the remainder is not larger than $\varepsilon^{5/2}$. Although we have not proven it, we suspect that this remainder is actually of order ε^3. The error estimate $\mathcal{O}(\varepsilon^{5/2})$ in (6.9) can indeed be improved, either by pushing the matching asymptotic expansions to the next order (which will likely deliver the next-order correction proportional to ε^3 in explicit form) or by changing the scaling assumption $i = \mathcal{O}(\varepsilon^{-1/2})$ used in the boundary layer to $i = \mathcal{O}(\varepsilon^{-1+h})$, where $h > 0$ is an arbitrarily small, positive number (which will likely show that the remainder in (6.9) is $\mathcal{O}(\varepsilon^{3-h'})$ for *any* $h' > 0$). This postulate is also supported by the numerical convergence analysis in Figure 8.3 (datapoints in red).

Remark 6.2. We have not included the additional matching conditions labelled i^4 and i^3 in (6.6) in the boundary-value problem (3.7) as they are redundant. Indeed, the forthcoming analysis in Sections 7–8 shows that the boundary conditions (6.8–6.9) suffice to make the solution $u_\varepsilon(x)$ regular, in the sense that the k-th derivative remains finite, $u_\varepsilon^{(k)}(x) = \mathcal{O}(\varepsilon^0)$, for any differentiation order $k \geqslant 0$. Differentiating the homogenized equation of equilibrium $(3.7)_1$ k times, assuming that the loading is smooth, and multiplying by $\varepsilon^{1+k/2}$, we get $\varepsilon^{1+k/2}(K u_\varepsilon^{(k+2)}(x) + \bar{f}^{(k)}(x)) = \mathcal{O}(\varepsilon^{3+k/2})$, which for $k = 2$ and $k = 1$ implies the matching condition labelled i^4 and i^3 in (6.6), respectively.

6.2. Matching about second endpoint $x = L$

The boundary layer analysis and the matching procedure are exactly similar at the other endpoint. A mirror-symmetry about the center of the lattice transforms the node labelled $(i, \pm)$ into that labelled $(N-i, \mp)$ and in particular, the endpoints are transformed into one another. The effective boundary conditions applicable at $x = L$ can therefore be derived readily by looking at the lattice 'in a mirror'. Noting that the mirror symmetry changes $(k_0, k_1, k_2, k_3, k_4)$ into $(k_L, k_1, k_2, k_4, k_3)$, x into $L - x$, and $u(x)$ into $-u(L-x)$, we conclude that the boundary conditions applicable at $x = L$ are those announced in (3.7), with

$$\begin{aligned} \ell_L &= -\ell^\dagger\Big(\frac{k_L}{k_1}, \frac{k_2}{k_1}, \frac{k_4}{k_1}, \frac{k_3}{k_1}\Big) \\ \tilde{\ell}_L &= +\tilde{\ell}^\dagger\Big(\frac{k_L}{k_1}, \frac{k_2}{k_1}, \frac{k_4}{k_1}, \frac{k_3}{k_1}\Big), \end{aligned} \tag{6.10}$$

where $\ell^\dagger$ and $\tilde{\ell}^\dagger$ are the functions yielding the constants $\ell_0 = \ell^\dagger(k_0/k_1, k_2/k_1, k_3/k_1, k_4/k_1)$ and $\ell_0 = \tilde{\ell}^\dagger(k_0/k_1, k_2/k_1, k_3/k_1, k_4/k_1)$ in the left-hand side boundary-layer in terms of the elastic contrasts. These functions are derived in closed analytical form in the companion notebook [Thb24]. With the values of the stiffness contrasts listed in Table 2.1, we obtain

$$\begin{aligned} \ell_L &\approx 0.691 \\ \tilde{\ell}_L &\approx 0.165. \end{aligned} \tag{6.11}$$

6.3. Uniform approximation of the nodal displacement

By matching the solutions (6.2) and (6.5) in the boundary layer near $x=0$, we have ensured that the polynomial terms proportional to i^0, …, $i^4/24$ in the boundary layer solution $\boldsymbol{V}_i^{\mathrm{BL}}$ in (6.5) sum up to yield the homogenized solution $\boldsymbol{V}_i^{\mathrm{int}}$ in (4.8). The only other term in (6.5) is the exponentially decreasing one. We can therefore rewrite the boundary layer solution (6.5) as

$$\boldsymbol{V}_i^{\mathrm{BL}} = \zeta^{-i}\left(\rho_0\,\varepsilon\,u_\varepsilon'(0)+\varepsilon^2\frac{\chi_0}{K}\bar{f}(0)\right)\boldsymbol{\Lambda}_0+\left[u_\varepsilon(\varepsilon i)\,\boldsymbol{W}_0+\varepsilon\,u_\varepsilon'(\varepsilon i)\,\boldsymbol{W}_1+\varepsilon^2 u_\varepsilon''(\varepsilon i)\,\boldsymbol{W}_2\right]+\mathcal{O}(\varepsilon^{5/2}). \tag{6.12}$$

where we have used the value of C_3 found in (6.7). The terms in square bracket are nothing but the homogenized solution $\boldsymbol{V}_i^{\mathrm{int}}$. Being derived from the boundary layer solution (6.5), this expression is valid in the boundary layer, for $i=\mathcal{O}(\varepsilon^{-1/2})$.

It turns out to be valid in the outer region as well: there, the exponential term becomes negligible, leaving only the homogenized $\boldsymbol{V}_i^{\mathrm{int}}$ in square brackets, and Equation (4.8) is recovered. We conclude that the following approximation is valid in both the boundary layer near $x=0$ and in the outer region,

$$\boldsymbol{V}_i = \begin{pmatrix} \zeta^{-i}\left(\rho_0\,\varepsilon\,u_\varepsilon'(0)+\varepsilon^2\frac{\chi_0}{K}\bar{f}(0)\right)\boldsymbol{\Lambda}_0 \\ \quad+\left[u_\varepsilon(\varepsilon i)\,\boldsymbol{W}_0+\varepsilon\,u_\varepsilon'(\varepsilon i)\,\boldsymbol{W}_1+\varepsilon^2 u_\varepsilon''(\varepsilon i)\,\boldsymbol{W}_2\right] \end{pmatrix} + \begin{cases} \mathcal{O}(\varepsilon^{5/2}) \text{ if } i=O(\varepsilon^{-1/2}) \\ \mathcal{O}(\varepsilon^{3}) \text{ if } i\gg 1 \text{ and } N-i\gg 1. \end{cases} \tag{6.13}$$

By a similar argument, this approximation can be extended to the other boundary layer near $x=L$ by adding a second exponential contribution. This yields the following *uniform* approximation, valid over the entire domain,

$$\boldsymbol{V}_i = \begin{pmatrix} \zeta^{-i}\left(\rho_0\,\varepsilon\,u_\varepsilon'(0)+\varepsilon^2\frac{\chi_0}{K}\bar{f}(0)\right)\boldsymbol{\Lambda}_0 \\ \quad+\zeta^{-(N-i)}\left(-\rho_L\,\varepsilon\,u_\varepsilon'(L)+\varepsilon^2\frac{\chi_L}{K}\bar{f}(L)\right)\boldsymbol{\Lambda}_L \\ \quad+\left[u_\varepsilon(\varepsilon i)\,\boldsymbol{W}_0+\varepsilon\,u_\varepsilon'(\varepsilon i)\,\boldsymbol{W}_1+\varepsilon^2 u_\varepsilon''(\varepsilon i)\,\boldsymbol{W}_2\right] \end{pmatrix} + \begin{cases} \mathcal{O}(\varepsilon^{5/2}) \text{ if } i=O(\varepsilon^{-1/2}) \\ \mathcal{O}(\varepsilon^{3}) \text{ if } i\gg 1 \text{ and } N-i\gg 1 \\ \mathcal{O}(\varepsilon^{5/2}) \text{ if } N-i=O(\varepsilon^{-1/2}). \end{cases} \tag{6.14}$$

The constants $\rho_L\approx 0.119$, $\chi_L\approx 0.0149$ and the vector $\boldsymbol{\Lambda}_L\approx\begin{pmatrix}1 & -2.65\end{pmatrix}$ are found by analyzing the boundary layer near $x=L$ and are akin to ρ_0, χ_0, $\boldsymbol{\Lambda}_0$.

Remark 6.3. Taking $i=0$ in (6.14), we obtain the displacement of the first node $v_{\bar{0}}=[\boldsymbol{V}_0]_1$ in the form

$$\begin{aligned} v_{\bar{0}} &= \left(\rho_0\,\varepsilon\,u_\varepsilon'(0)+\varepsilon^2\chi_0\frac{\bar{f}(0)}{K}\right)[\boldsymbol{\Lambda}_0]_1+u_\varepsilon(0)\,[\boldsymbol{W}_0]_1+\varepsilon\,u_\varepsilon'(0)\,[\boldsymbol{W}_1]_1+\varepsilon^2 u_\varepsilon''(0)\,[\boldsymbol{W}_2]_1+\mathcal{O}(\varepsilon^{5/2}) \\ &= u_\varepsilon(0)\,[\boldsymbol{W}_0]_1+\varepsilon\,u_\varepsilon'(0)\,(\rho_0\,[\boldsymbol{\Lambda}_0]_1+[\boldsymbol{W}_1]_1)+\varepsilon^2 u_\varepsilon''(0)\,(-\chi_0\,[\boldsymbol{\Lambda}_0]_1+[\boldsymbol{W}_2]_1)+\mathcal{O}(\varepsilon^{5/2}), \end{aligned} \tag{6.15}$$

where $[\boldsymbol{x}]_1$ denotes the first component of the vector $\boldsymbol{x}$. Identifying with the kinematic boundary condition $v_{\bar{0}}=v_{\bar{0}}^\star$ in (6.9), we obtain the following relations between the boundary layer constants: $\rho_0\,[\boldsymbol{\Lambda}_0]_1+[\boldsymbol{W}_1]_1=0.119\times(-8.34)-3/8=-1.37=\ell_0$ and $-\chi_0\,[\boldsymbol{\Lambda}_0]_1+[\boldsymbol{W}_2]_1=-0.0149\times(-8.34)+0=+0.124=\tilde{\ell}_0$. By a similar argument, the constants in the other boundary layer are related by $-\rho_L\,[\boldsymbol{\Lambda}_L]_2+[\boldsymbol{W}_1]_2=\ell_L$ and $-\chi_L\,[\boldsymbol{\Lambda}_L]_2+[\boldsymbol{W}_2]_2=\tilde{\ell}_L$.

7. PERTURBATIVE SOLUTION TO THE BOUNDARY-VALUE PROBLEM

In this section, we solve the boundary-value problem (3.7) perturbatively, taking advantage of the fact that the asymptotically correct boundary conditions inhibit short-wavelength oscillations. We point out that this perturbative approach breaks down if the *ad hoc* boundary conditions (3.5) are used instead.

We denote as $u_{[k]}(x)$ the order-ε^k approximation of the macroscopic displacement, obtained by truncating the infinite-series solution $u_\varepsilon(x)$ in (4.2) at order ε^k,

$$u_{[k]}(x) \coloneqq u_{(0)}(x)+\cdots+\varepsilon^k u_{(k)}(x), \tag{7.1}$$

In our notation, we use *parentheses* in subscript for a contribution of order ε^k as in (4.2), and *square brackets* in subscript for a series truncated at order ε^k as in (7.1).

The successive approximations $u_{[k]}$'s are found by solving the boundary-value problem (3.7) order by order in ε: $u_{[0]}$, $u_{[1]}$ and $u_{[2]}$ are accurate to ε^0, ε^1, and ε^2 included, respectively.

Order 0 The leading order solution $u_{[0]}(x)=u_{(0)}(x)$ satisfies the classical equilibrium for an elastic bar, $Ku_{[0]}''(x)+\bar{f}(x)=0$, along with the kinematic boundary conditions $u_{[0]}(0)=v_0^\star$ and $u_{[0]}(L)=v_L^\star$. The solution is

$$u_{[0]}(x)=a_0\frac{x}{L}+b_0-\frac{1}{K}\bar{f}^{(-2)}(x) \tag{7.2}$$

where

$$\begin{aligned} a_0 &= v_L^\star-v_0^\star+\frac{1}{K}\bar{f}^{(-2)}(L) \\ b_0 &= v_0^\star. \end{aligned} \tag{7.3}$$

Here, $\bar{f}^{(-2)}(x)$ is the double primitive of $\bar{f}(x)$ satisfying $\bar{f}^{(-2)}(0)=0$ and $\bar{f}^{(-2)\prime}(0)=0$, given by the explicit formula

$$\bar{f}^{(-2)}(x)=\int_0^x\left(\int_0^{x'}\bar{f}(x'')\,\mathrm{d}x''\right)\mathrm{d}x'. \tag{7.4}$$

Order 1 The first-order correction is the solution of $Ku''_{(1)}(x)=0$ with the boundary conditions $u_{(1)}(0)=-\ell_0 u'_{[0]}(0)=-\ell_0 a_0/L$ and $u_{(1)}(L)=-\ell_L u'_{(0)}(L)=-\ell_L\left(a_0/L-\bar{f}^{(-2)\prime}(L)/K\right)$, which yields

$$u_{(1)}(x)=a_1\frac{x}{L}+b_1 \tag{7.5}$$

with

$$\begin{aligned} a_1 &= \left(-\frac{(\ell_L-\ell_0)\,a_0}{L}+\frac{\ell_L}{K}\bar{f}^{(-2)\prime}(L)\right)\\ b_1 &= -\frac{a_0\,\ell_0}{L}. \end{aligned} \tag{7.6}$$

The order-ε approximation $u_{[1]}(x)=u_{[0]}(x)+\varepsilon u_{(1)}(x)$ is therefore given by

$$u_{[1]}(x)=\alpha_{[1]}\frac{x}{L}+\beta_{[1]}-\frac{1}{K}\bar{f}^{(-2)}(x) \tag{7.7}$$

where $\alpha_{[1]}=a_0+\varepsilon a_1$ and $\beta_{[1]}=b_0+\varepsilon b_1$.

Order 2 The second-order correction satisfies $Ku''_{(2)}(x)=Bu''''_{[0]}(x)$ with the kinematic boundary conditions $u_{(2)}(0)=-\ell_0 u'_{(1)}(0)-\tilde{\ell}_0 u''_{[0]}(0)$ and $u_{(2)}(L)=-\ell_L u'_{(1)}(L)-\tilde{\ell}_L u''_{[0]}(L)$. The solution is

$$u_{(2)}(x)=a_2\frac{x}{L}+b_2-\frac{B}{K^2}\bar{f}(x), \tag{7.8}$$

where

$$\begin{aligned} a_2 &= \left(-\frac{(\ell_L-\ell_0)}{L}a_1+\frac{(B+K\tilde{\ell}_L)}{K^2}\bar{f}(L)-\frac{(B+K\tilde{\ell}_0)}{K^2}\bar{f}(0)\right)\\ b_2 &= -a_1\frac{\ell_0}{L}+\frac{(B+K\tilde{\ell}_0)}{K^2}\bar{f}(0) \end{aligned} \tag{7.9}$$

We must also consider the static boundary conditions $\varepsilon^2\left(Ku''_\varepsilon+\bar{f}\right)_{x=0,L}=0$ that appear at order ε^2 in (3.7). At this order, they can be simplified as

$$\left(Ku''_{[0]}+\bar{f}\right)_{x=0,L}=0. \tag{7.10}$$

Being redundant with the leading-order equilibrium in the bulk, they are automatically satisfied, as can be checked by inserting the expression (7.2) of $u_{[0]}(x)$ into (7.10). We therefore have 4 boundary conditions overall for the second-order ordinary differential equation for $u_{(2)}(x)$, which is too much, but 'luckily' the 2 supernumerary boundary conditions are automatically satisfied.

The order-ε^2 approximation $u_{[2]}(x)=u_{[1]}(x)+\varepsilon^2 u_{(2)}(x)$ is thus given by

$$u_{[2]}(x)=\alpha_{[2]}\frac{x}{L}+\beta_{[2]}-\frac{1}{K}\bar{f}^{(-2)}(x)-\frac{B}{K^2}\varepsilon^2\bar{f}(x), \tag{7.11}$$

where $\alpha_{[2]}=a_0+\varepsilon a_1+\varepsilon^2 a_2$ and $\beta_{[2]}=b_0+\varepsilon b_1+\varepsilon^2 b_2$.

These successive approximations are consistent with the direct (non-perturbative) solution of the boundary-value problem (3.7) derived in Appendix A, see the discussion following Equation (8.7).

Remark 7.1. With the *ad hoc* boundary conditions (3.5), the supernumerary boundary conditions (7.10) become $\left(Ku''_{[0]}\right)_{x=0,L}=0$: they are in conflict with the leading-order solution that satisfies $\left(Ku''_{[0]}+\bar{f}\right)_{x=0,L}=0$, except in the special circumstance where the applied load vanishes at both endpoints, $\bar{f}(0)=\bar{f}(L)=0$. The perturbative expansion therefore breaks down at order ε^2 due to the spurious short-wavelength oscillations discussed in Section 3.2.

Remark 7.2. In view of (7.2), the perturbation problem at order ε^2 can be rewritten as $Ku''_{(2)}(x)=Bu''''_{[0]}(x)=-B\bar{f}''(x)/K$. Due to the presence of a second derivative $\bar{f}''$ in the right-hand side, it requires more severe smoothness conditions on the distributed load $\bar{f}(x)$ than the leading-order problem, $Ku''_{[0]}(x)=-\bar{f}(x)$. The perturbative expansion may therefore break down if the load is insufficiently smooth, which points to the presence of *loading-induced* inner layers. Such layers require a special treatment, similar to that of the boundary layers, see Section 5. We limit attention to infinitely smooth loading.

8. NUMERICAL VALIDATION

We validate the predictions of the effective model (3.7) by comparing to numerical solutions of the discrete lattice. To this end, we use a cubic loading profile $\bar{f}(x)$ and clamped boundary conditions on both sides,

$$\bar{f}(x)=\frac{k_1}{L}\left(\frac{x}{L}\right)^3 f^\star,\quad v_0^\star=0,\quad v_L^\star=0.1\,L. \tag{8.1}$$

Our goal is to establish the order of accuracy of the continuous model in the limit of a fine lattice, $\varepsilon\to 0$.

8.1. Predicted nodal displacement

We start by calculating the nodal displacements $\boldsymbol{V}_i=(\,v_i^-\;\;v_i^+\,)$ predicted by our method. For the cubic loading profile in (8.1), the second primitive is given by $\bar{f}^{(-2)}(x)=k_1 L f^\star(x/L)^5/20$ and the general solution at order ε^2 derived in (7.11) takes the form

$$u_{[2]}(x)=\alpha_{[2]}\frac{x}{L}+\beta_{[2]}-\frac{f^\star L k_1}{20K}\left(\frac{x}{L}\right)^5-\frac{Bk_1 f^\star\varepsilon^2}{K^2 L}\left(\frac{x}{L}\right)^3. \tag{8.2}$$

Inserting this into the composite approximation (6.14), we obtain an approximation of the nodal displacement at order ε^2 as

$$\boldsymbol{V}_i^{[2]} = \left(\begin{array}{l} \zeta^{-i} \left(\rho_0 \varepsilon u'_{[2]}(0) + \varepsilon^2 \dfrac{\chi_0}{K} \bar{f}(0) \right) \boldsymbol{\Lambda}_0 \\ \quad + \zeta^{-(N-i)} \left(-\rho_L \varepsilon u'_{[2]}(L) + \varepsilon^2 \dfrac{\chi_L}{K} \bar{f}(L) \right) \boldsymbol{\Lambda}_L \\ \quad + \left[u_{[2]}(\varepsilon i)\, \boldsymbol{W}_0 + \varepsilon u'_{[2]}(\varepsilon i)\, \boldsymbol{W}_1 + \varepsilon^2 u''_{[2]}(\varepsilon i)\, \boldsymbol{W}_2 \right] \end{array} \right). \tag{8.3}$$

This prediction is tested against solutions to the discrete lattice problem in the following subsections.

In these comparisons, we will also include the order-ε^0 and order-ε^1 approximations of the macroscopic displacement, see (7.2) and (7.7),

$$\begin{array}{rcl} u_{[0]}(x) & = & a_0 \dfrac{x}{L} + b_0 \quad - \dfrac{f^\star L k_1}{20K} \left(\dfrac{x}{L} \right)^5 \\ u_{[1]}(x) & = & a_{[1]} \dfrac{x}{L} + \beta_{[1]} - \dfrac{f^\star L k_1}{20K} \left(\dfrac{x}{L} \right)^5 \end{array} \tag{8.4}$$

and of the nodal displacements,

$$\begin{array}{rcl} \boldsymbol{V}_i^{[0]} & = & u_{[0]}(\varepsilon i)\, \boldsymbol{W}_0 \\ \boldsymbol{V}_i^{[1]} & = & \zeta^{-i} \rho_0 \varepsilon u'_{[1]}(0)\, \boldsymbol{\Lambda}_0 \; - \; \zeta^{-(N-i)} \rho_L \varepsilon u'_{[1]}(L)\, \boldsymbol{\Lambda}_L \; + \; u_{[1]}(\varepsilon i)\, \boldsymbol{W}_0 + \varepsilon u'_{[1]}(\varepsilon i)\, \boldsymbol{W}_1. \end{array} \tag{8.5}$$

8.2. Case of zero applied loading, $f^\star = 0$

We first consider the special case where no distributed load is applied, $f^\star = 0$ in (8.1). In this case, the lattice deforms exclusively as a result of the prescribed end displacement $v_L^\star = 0.1\,L$. The continuous solution $u_{[2]}(x) = a_{[2]} x/L + \beta_{[2]}$ is then an affine function of x, see (8.2) and the red line in Figure 8.1. Its leading-order approximation $u_{[0]}(x) = v_L^\star x/L$ is particularly simple and it is affine as well, see (8.4) and the green line in the figure. The strain gradient $u''_{[i]}(x) = 0$ is zero at all orders $0 \leqslant i \leqslant 2$, *i.e.*, there is no gradient effect in the bulk. Any error in the continuous model (revealed by the discrepancy between the colored elements and the discrete solution shown using the black and white symbols in the figure) must therefore be attributed to the effective boundary conditions. The leading-order effective boundary conditions, in particular, lead to a noticeable overestimation of the strain in the interior (slope of green curve is too high). This finite-length effect is enhanced by the moderate number of cells $N = 10$ used in the simulation (it becomes less and less significant in the limit $N \to \infty$) and by the relatively soft spring constants $k_0 = k_1$ and $k_L = k_0$ assigned to the terminal springs. Switching to the order-ε^1 model (blue crosses) decreases the error significantly. Similar results have been obtained with other models accounting for boundary effects at order ε^1 in 2D composites [Dum86]. The agreement is further improved with the order-ε^2 model (the red crosses match the black circles and disks almost perfectly).

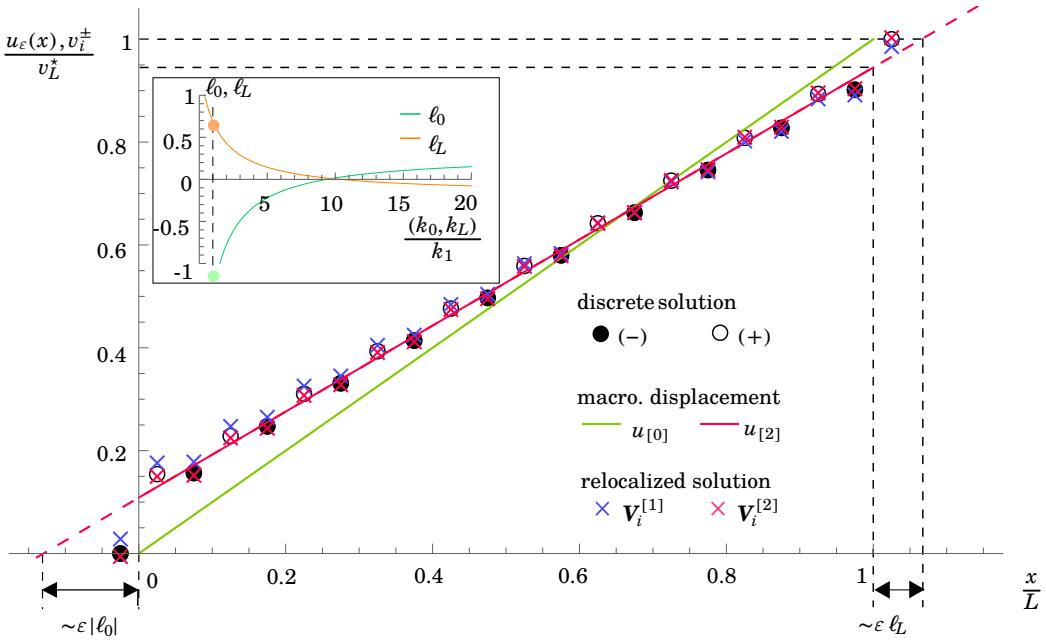

Figure 8.1. Comparison of the displacement predicted by the continuous model at order ε^0 (green), ε^1 (blue) and ε^2 (red) based on Equations (8.2–8.5), with the discrete solution to the lattice discrete problem for $N = 10$ (disk symbols). Both the macroscopic displacement u_ε is shown (solid lines) and the relocalized nodal positions $\boldsymbol{V}_i$ (crosses). The lattice is deformed by a displacement of the terminal node $v_L^\star = 0.1\,L$, no distributed load being applied ($f^\star = 0$). The spring constants listed in Table 2.1 are used. (*Inset*) Characteristic lengths ℓ_0 (resp. ℓ_L) entering in the effective boundary conditions as functions of the 'exceptional' spring constant k_0 (resp. k_L). The dashed vertical line corresponds to the values $k_0 = k_L = k_1$ used in the numerical illustrations and shown along the horizontal axis of the main plot.

In the absence of a distributed force, $\bar{f}(x) \equiv 0$, (and thus of a strain-gradient, $u_\varepsilon''(x) \equiv 0$), the second-order homogenized model (3.7) can be rewritten as

$$\begin{aligned} &K u_\varepsilon''(x) = 0 \quad \forall x \\ &\begin{cases} u_\varepsilon(\varepsilon\,\ell_0) = 0 \\ u_\varepsilon(L + \varepsilon\,\ell_L) = v_L^\star. \end{cases} \end{aligned} \tag{8.6}$$

This is nothing but a *classical* bar model covering the *extended* domain $\varepsilon\,\ell_0 \leqslant x \leqslant L + \varepsilon\,\ell_L$ and having thus an effective length $L_{\text{eff}} = L + \varepsilon\,(\ell_L - \ell_0) \neq L$. This change in length is the only aspect in which the higher-order effective model differs from the leading-order one in the absence of a distributed force. In the inset in Figure 8.1, the characteristic lengths ℓ_0 and ℓ_L are represented as functions of the spring constants k_0 and k_L of the terminal springs: as can be expected, the softer the exceptional springs, the larger the effective length $L_{\text{eff}} = L + \varepsilon\,(\ell_L - \ell_0)$.

The alternate form (8.6) of the boundary-value problem has a *direct* solution,

$$u_\varepsilon^{\text{d}}(x) = v_L^\star \frac{x - \varepsilon\,\ell_0}{L + \varepsilon\,(\ell_L - \ell_0)}. \tag{8.7}$$

By 'direct', we mean a non-perturbative solution—note the ε in the denominator. The successive approximations $u_{[0]}(x) = v_L^\star x/L$, $u_{[1]}(x) = \alpha_{[1]} x/L + \beta_{[1]}$ and $u_{[2]}(x) = \alpha_{[2]} x/L + \beta_{[2]}$ obtained earlier using the perturbation method are nothing but the Taylor expansions of $u_\varepsilon^{\text{d}}(x)$ in (8.7) to order ε^0, ε^1 and ε^2, respectively.

Remark 8.1. In the boundary-value problem (8.6), the higher-order corrections are irrelevant since they get multiplied by the higher-order derivatives $u_\varepsilon^{(p)} \equiv 0$ which are all zero for $p \geqslant 2$. This shows that the boundary-value problem (8.6) and its solution (8.7) are exact to any order in ε.

8.3. Effect of a distributed loading, $f^\star \neq 0$

We now include a distributed load and set $f^\star = 2$ in (8.1). Due to the gradient effect, the solution $u_{[2]}(x)$ in (8.2) has a corrective term proportional to $f^\star B\,\varepsilon^2\,(x/L)^3$, in addition to the classical term proportional to $f^\star\,(x/L)^5$. The relocalized solution $\boldsymbol{V}_i^{[2]}$ in (8.3) is plotted in Figure 8.2 for a discrete lattice comprising $N = 10$ cells, along with the leading-order macroscopic displacement $u_{[0]}(x)$ in (8.4) and the first-order relocalized solution $\boldsymbol{V}_i^{[1]}$ from (8.5). Except for the non-affine profile of the displacement, the results are similar to those obtained earlier in Figure 8.1 in the absence of a distributed force. The leading-order overestimates the stiffness of the terminal cells and makes poor predictions overall. The first-order solution is significantly more accurate but there are still noticeable systematic errors near the ends, for $x \leqslant 0.3$ and $x \geqslant 0.8$, coming from both the effective boundary conditions and from the neglect of the strain-gradient correction. The second-order solution can hardly be distinguished from the reference solution over the entire domain.

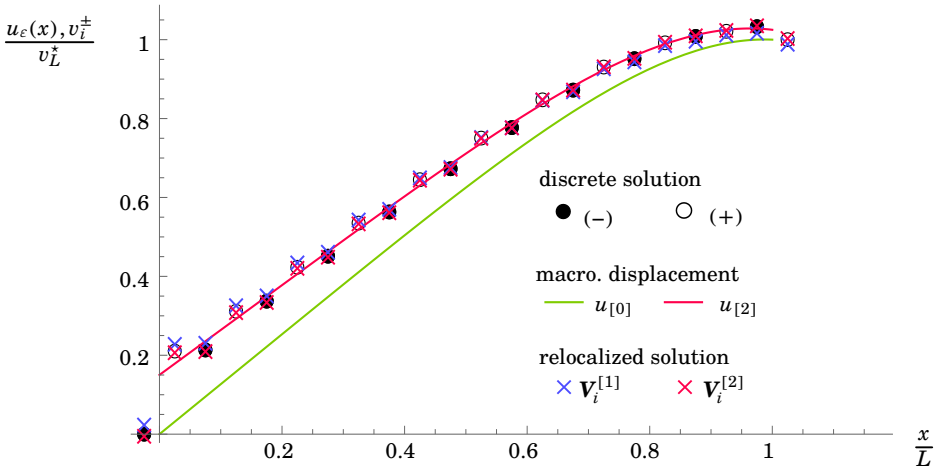

Figure 8.2. Comparison of the displacement predicted by the continuous model to the discrete solution of the lattice problem, with $N = 10$ cells and in the presence of a distributed force ($f^\star = 2$). Same conventions as in Figure 8.1.

The convergence analysis shown in Figure 8.3 quantifies the error. For different cells numbers N and with a fixed length $L = 1$, we compare the relocalized solutions $(\boldsymbol{V}_i^{[j]})_{0 \leqslant i \leqslant N}$ at order j in (8.3) and (8.5) to the reference solution $\boldsymbol{V}_i^{\text{ref}}$ obtained by solving the equilibrium of the discrete lattice. The error is measured by the quantity

$$e_{[j]}(N) = \left(\frac{1}{N\,(v_L^\star)^2} \sum_{i=0}^{N} \|\boldsymbol{V}_i^{[j]} - \boldsymbol{V}_i^{\text{ref}}\|^2 \right)^{1/2}. \tag{8.8}$$

In particular, the error in the solution generated by the boundary-value problem (3.7) is of order ε^3, as anticipated (red symbols). This is our main result. Achieving this order of accuracy requires both second-order homogenization in the interior of the domain, and second-order-accurate boundary conditions.

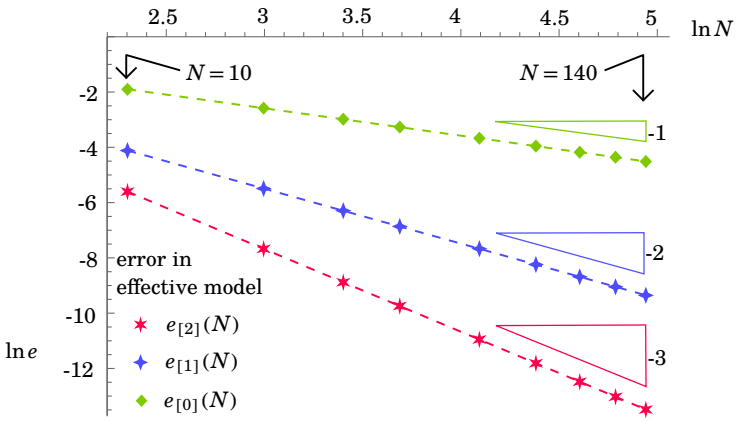

Figure 8.3. Convergence analysis: the error $e_{[j]}(N)$ obtained by comparing the prediction $\boldsymbol{V}_i^{[j]}$ of the effective model of order j with the reference, discrete solution $\boldsymbol{V}_i^{\text{ref}}$ is plotted as a function of the number of cells $N = \varepsilon^{-1}$ ($L = 1$) in a log-log plot (natural log). A distributed force $f^\star = 2$ is applied. The convergence rates indicated by the triangles are consistent with the fact that the order-ε^j model makes an error $\mathcal{O}(\varepsilon^{j+1})$.

9. CONCLUSION AND PERSPECTIVES

We have derived a higher-order, continuous bar model for a one-dimensional lattice of springs, along with effective boundary conditions representing the boundary layers forming at the endpoints. Both are accurate to order ε^2 included, where ε is the scale separation parameter. The equilibrium of the higher-order bar model has been formulated as a boundary-value problem. For smooth applied loading, the solutions of the boundary-value problem have been checked to agree with the equilibria of the discrete lattice up to an error of order ε^3.

Homogenization of a one-dimensional lattice of springs delivers the following sequence of models. At leading order, a differential equation of order 2 is obtained, along with a single boundary condition at each endpoint (classical bar model). First-order homogenization is similar: the boundary conditions get refined but their number stays the same and the differential equation is unchanged. In this work, we have focussed on second-order homogenization which is markedly different, much less explored and also more challenging: the order of the differential equation increases to 4 (higher-order bar model) and a second boundary condition is needed at each endpoint. We have derived asymptotically correct boundary conditions and have pointed out their remarkable property: they suppress the undesirable, short-wavelength oscillations that are present in the general solution of the higher-order bar model. These oscillations contradict the basic assumptions underpinning homogenization. Using these particular boundary conditions is therefore essential not only for accuracy but also for consistency.

Higher-order homogenization is known to produce negative gradient moduli not only with one-dimensional lattices but also more broadly with both periodic lattices or periodic continua in dimensions two and three. One of the issues raised by these negative moduli is the presence of short-wavelength oscillations. Based on the example of the one-dimensional lattice, we have shown that the oscillations are removed by a careful analysis of the boundaries. Another important issue raised by the presence of negative moduli is the non-positivity of the homogenized energy. We will address this important remaining issue in a follow-up paper—the present work suggests that the boundaries are the key to restore the positivity of the energy.

With the asymptotically correct boundary conditions, a perturbative solution strategy is possible, as we have pointed out. It entails solving a sequence of *second-order* differential equations whose left-hand sides (elasticity operators) are identical to that of the classical bar model: the gradient effect is taken into account perturbatively in the right-hand sides. The perturbative approach is promising for future numerical simulations of homogenized models of periodic continua in 2D or 3D : unlike fourth-order partial differential equations whose implementation by the finite-element method requires high-order elements, the second-order equations delivered by the perturbative approach can be readily implemented using classical numerical models and are associated with a positive energy.

The one-dimensional lattice analyzed in this paper is simple enough that it could be homogenized to second order in closed analytical form. Doing so led to the same difficulties that are faced with more complex periodic structures, namely the presence of negative gradient stiffness causing short-wavelength oscillations. Taking advantage of the explicit mathematical formula, we could diagnose and remedy some of these issues, and obtain a boundary-value problem that delivers accurate approximations to the discrete problem. By showing that one can live with negative gradient stiffness, our work will hopefully help high-order homogenized models gain the popularity they deserve.

Acknowledgements This manuscript has been typeset using TEXMACS, a powerful, multi-platform and freely distributed scientific editor [vdHGG+13].

BIBLIOGRAPHY

[A77] J. L. Auriault and É. Sanchez-Palencia. Etude du comportement macroscopique d'un milieu poreux saturé déformable. *J Mec*, 16:575–603, 1977.

[AA99] G. Allaire and M. Amar. Boundary layer tails in periodic homogenization. *ESAIM: Control, Optimisation and Calculus of Variations*, 4:209–243, 1999.

[ABV16] G. Allaire, M. Briane, and M. Vanninathan. A comparison between two-scale asymptotic expansions and Bloch wave expansions for the homogenization of periodic structures. *SeMA Journal*, 73(3):237–259, 2016.

[ACM98] R. Abdelmoula, M. Coutris, and J. J. Marigo. Comportement asymptotique d'une interphase élastique mince. *Comptes Rendus de l'Académie des Sciences - Series IIB - Mechanics-Physics-Chemistry-Astronomy*, 326(4):237–242, 1998.

[AL23] B. Audoly and C. Lestringant. An energy approach to asymptotic, higher-order, linear homogenization. *Journal of Theoretical, Computational and Applied Mechanics*, page 11414, 2023.

[AMPB08] H. Askes, A.V. Metrikine, A.V. Pichugin, and T. Bennett. Four simplified gradient elasticity models for the simulation of dispersive wave propagation. *Philosophical Magazine*, 88(28-29):3415–3443, 2008.

[BLP11] A. Bensoussan, J. L. Lions, and G. Papanicolaou. *Asymptotic Analysis for Periodic Structures*, volume 374. American Mathematical Soc., 2011.

[BMP21] A. L. Baldelli, J. J. Marigo, and C. Pideri. Analysis of boundary layer effects due to usual boundary conditions or geometrical defects in elastic plates under dending: an improvement of the Love–Kirchhoff model. *Journal of Elasticity*, 143(1):31–84, 2021.

[BO99] C. M. Bender and S. A. Orszag. Boundary-Layer Theory. In *Advanced mathematical methods for scientists and engineers I: Asymptotic methods and perturbation theory*, pages 419–483. Springer, New York, NY, 1999.

[Bou72] J. Boussinesq. Théorie des ondes et des remous qui se propagent le long d'un canal rectangulaire horizontal, en communiquant au liquide contenu dans ce canal des vitesses sensiblement pareilles de la surface au fond. *Journal de Mathématiques Pures et Appliquées*, pages 55–108, 1872.

[Bou96] C. Boutin. Microstructural effects in elastic composites. *International Journal of Solids and Structures*, 33(7):1023–1051, 1996.

[Bou20] C. Boutin. Homogenization methods and generalized continua in linear elasticity. In H. Altenbach and A. Öchsner, editors, *Encyclopedia of continuum mechanics*. Springer, Berlin, Heidelberg, 2020.

[BP89] N. Bakhvalov and G. Panasenko. *Homogenisation: Averaging Processes in Periodic Media*, volume 36 of *Mathematics and Its Applications*. Springer Netherlands, Dordrecht, 1989.

[BS11] C. Boutin and J. Soubestre. Generalized inner bending continua for linear fiber reinforced materials. *International Journal of Solids and Structures*, 48(3):517–534, 2011.

[CC09] E. Cosserat and F. Cosserat. Théorie des corps déformables. *Nature*, 81(2072):67–67, 1909.

[CT02] M. Charlotte and L. Truskinovsky. Linear elastic chain with a hyper-pre-stress. *Journal of the Mechanics and Physics of Solids*, 50(2):217–251, 2002.

[DLSS22] B. Durand, A. Lebée, P. Seppecher, and K. Sab. Predictive strain-gradient homogenization of a pantographic material with compliant junctions. *Journal of the Mechanics and Physics of Solids*, 160:104773, 2022.

[Dum86] H. Dumontet. Study of a boundary layer problem in elastic composite materials. *ESAIM: Mathematical Modelling and Numerical Analysis*, 20(2):265–286, 1986.

[Eck73] W. Eckhaus. *Matched asymptotic expansions and singular perturbations*, volume 6. North Holland, Amsterdam, New York, 1973.

[FF+22] M. Fergoug, A. Parret-Fréaud, N. Feld, B. Marchand, and S. Forest. A general boundary layer corrector for the asymptotic homogenization of elastic linear composite structures. *Composite Structures*, 285:115091, 2022.

[Ger73] P. Germain. La méthode des puissances virtuelles en mécanique des milieux continus, premiere partie: théorie du second gradient. *J. Mécanique*, 12(2):235–274, 1973.

[GK89] B. Gambin and E. Kröner. Higher-order terms in the homogenized stress-strain relation of periodic elastic media. *Physica status solidi (b)*, 151(2):513–519, 1989.

[H74] H. P. Huy and E. Sanchez-Palencia. Phénomènes de transmission à travers des couches minces de conductivitéélevée. *Journal of Mathematical Analysis and Applications*, 47(2):284–309, 1974.

[Ili92] A. M. Ilin. *Matching of asymptotic expansions of Solutions of boundary value problems*. American Mathematical Society, UK ed. edition, 1992.

[KMU19] S. Koley, P. M. Mohite, and C. S. Upadhyay. Boundary layer effect at the edge of fibrous composites using homogenization theory. *Composites Part B: Engineering*, 173:106815, 2019.

[KP09] J.D. Kaplunov and A.V. Pichugin. On rational boundary conditions for higher-order long-wave models. In F.M. Borodich, editor, *IUTAM Symposium on Scaling in Solid Mechanics*, Iutam Bookseries, pages 81–90. Dordrecht, 2009. Springer Netherlands.

[KZ64] M. D. Kruskal and N. J. Zabusky. Stroboscopic-perturbation procedure for treating a class of nonlinear wave equations. *Journal of Mathematical Physics*, 5:231–244, 1964.

[Lag88] P. A. Lagerstrom. *Matched asymptotic expansions: ideas and techniques*, volume 76 of *Applied Mathematical Sciences*. Springer, New York, NY, 1988.

[LM18] D. T. Le and J. J. Marigo. Second order homogenization of quasi-periodic structures. *Vietnam Journal of Mechanics*, 40(4):325–348, 2018.

[Min64] R. D. Mindlin. Micro-structure in linear elasticity. *Archive for Rational Mechanics and Analysis*, 16(1):51–78, 1964.

[Ros86] P. Rosenau. Dynamics of nonlinear mass-spring chains near the continuum limit. *Physics Letters A*, 118(5):222–227, 1986.

[S18a] H. Abdoul-Anziz and P. Seppecher. Homogenization of periodic graph-based elastic structures. *Journal de l'École polytechnique-Mathématiques*, 5:259–288, 2018.

[S18b] H. Abdoul-Anziz and P. Seppecher. Strain gradient and generalized continua obtained by homogenizing frame lattices. *Mathematics and Mechanics of Complex Systems*, 6(3):213–250, 2018.

[San80] E. Sanchez-Palencia. *Non-homogeneous media and vibration theory*, volume 127 of *Lecture Notes in Physics*. Springer, Berlin, Heidelberg, 1980.

[San86] E. Sanchez-Palencia. Homogenization in mechanics. A survey of solved and open problems. 44(1):1–45, 1986.
[SC00] V P Smyshlyaev and K D Cherednichenko. On rigorous derivation of strain gradient effects in the overall behaviour of periodic heterogeneous media. 2000.
[TB93] N. Triantafyllidis and S. Bardenhagen. On higher order gradient continuum theories in 1-D nonlinear elasticity. Derivation from and comparison to the corresponding discrete models. 1993.
[TB96] N. Triantafyllidis and S. Bardenhagen. The influence of scale size on the stability of periodic solids and the role of associated higher order gradient continuum models. *Journal of the Mechanics and Physics of Solids*, 44(11):1891–1928, 1996.
[Thb24] M. Thbaut. https://archive.softwareheritage.org/browse/origin/https://git.renater.fr/anonscm/git/manon-thbaut-pb/manon-thbaut-pb.git. 2024.
[Tou62] R. A. Toupin. Elastic materials with couple-stresses. *Archive for Rational Mechanics and Analysis*, 11(1):385–414, jan 1962.
[vdHGG+13] J. van der Hoeven, A. Grozin, M. Gubinelli, G. Lecerf, F. Poulain, and D. Raux. GNU TEXmacs: a scientific editing platform. *ACM Communications in Computer Algebra*, 47(1–2):59–61, 2013.
[Vin16] V. Vinoles. *Problèmes d'interface en présence de métamatériaux: modélisation, analyse et simulations*. PhD thesis, Université Paris Saclay (COmUE), 2016.
[Wol21] Wolfram Research Inc. Mathematica, Version 13.0.0. 2021. Champaign, IL, 2021.
[YAL24] Y. Ye, B. Audoly, and C. Lestringant. Asymptotic, second-order homogenization of linear elastic beam networks. *Journal of the Mechanics and Physics of Solids*, 188:105637, 2024.

APPENDIX A. AMPLITUDE OF THE SHORT-SCALE OSCILLATIONS

In this Appendix, we combine the general solution (3.6) to the homogenized equation of equilibrium (3.1) with two sets of boundary conditions. We show that the undesirable, short-wavelength oscillations included in this general solution go away when the asymptotically correct boundary conditions are used (Section A.1), but remain present when the *ad hoc* boundary conditions are used (Section A.2).

In either case, we start from the expression (3.6) of the general solution to the homogenized equilibrium equation, which we now denote as $u_{\text{gen}}(x)$:

$$u_{\text{gen}}(x) = D_1 \sin\Big(\frac{\omega x}{\varepsilon}\Big) + D_2 \cos\Big(\frac{\omega x}{\varepsilon}\Big) + D_3 x + D_4 - \frac{1}{K}\bar{f}^{(-2)}(x) - \frac{B}{K^2}\varepsilon^2 \bar{f}(x), \tag{A.1}$$

where $\omega = \sqrt{K/(-B)}$. For any choice of the constants $(D_i)_{1\leqslant i\leqslant 4}$, it solves the differential equation

$$K u''_{\text{gen}}(x) - \varepsilon^2 B\, u''''_{\text{gen}}(x) + \bar{f}(x) = \varepsilon^4 \frac{B^2}{K^2} \bar{f}''''(x). \tag{A.2}$$

The right-hand side is of order ε^4, beyond what the effective model resolves, warranting consistency with the homogenized equation (3.1).

A.1. Using the asymptotic higher-order boundary conditions

Inserting the general solution (A.2) into the asymptotic boundary condition $K u''_{\text{gen}}(L) + \bar{f}(L) = 0$ in $(3.7)_5$ we get

$$-K\omega^2\varepsilon^{-2}\left(D_1 \sin\Big(\frac{\omega L}{\varepsilon}\Big) + D_2 \cos\Big(\frac{\omega L}{\varepsilon}\Big)\right) = \varepsilon^2 \frac{B}{K}\bar{f}''(L). \tag{A.3}$$

Similarly, the other boundary condition $K u''_{\text{gen}}(0) + \bar{f}(0) = 0$ in $(3.7)_3$ yields

$$-K\omega^2\varepsilon^{-2} D_2 = \varepsilon^2 \frac{B}{K}\bar{f}''(0). \tag{A.4}$$

Ignoring the exceptional case where ωL is a multiple of $\varepsilon\pi$, we get from Equations (A.3–A.4)

$$(D_1, D_2) = \mathcal{O}(\varepsilon^4). \tag{A.5}$$

Their amplitude is beyond the order ε^2 which we are resolving, meaning that the oscillatory terms are effectively suppressed.

A.2. Using the *ad-hoc* boundary conditions

When the *ad hoc* boundary conditions in (3.5) are used, Equations (A.3–A.4) are modified respectively to

$$-K\omega^2\varepsilon^{-2}\left(D_1 \sin\Big(\frac{\omega L}{\varepsilon}\Big) + D_2 \cos\Big(\frac{\omega L}{\varepsilon}\Big)\right) = -\bar{f}(L) + \varepsilon^2 \frac{B}{K}\bar{f}''(L) \tag{A.6}$$

and

$$-K\omega^2\varepsilon^{-2} D_2 = -\bar{f}(0) + \varepsilon^2 \frac{B}{K}\bar{f}''(0). \tag{A.7}$$

The new terms $-\bar{f}$ in the right-hand sides arise from the incompatibility with the equilibrium in the bulk (3.1). In this case, we get much larger amplitudes,

$$(D_1, D_2) = \mathcal{O}(\varepsilon^2). \tag{A.8}$$

The oscillatory terms $D_1 \sin(\omega x/\varepsilon)$ and $D_2 \cos(\omega x/\varepsilon)$ then contribute to the homogenized equilibrium (3.1) at order $\varepsilon^2 B D_i \varepsilon^{-4} \sim \varepsilon^0$: their contributions are *dominant*, which is inconsistent as these terms have been introduced as small corrections in a first place.

APPENDIX B. DETAILS OF THE HOMOGENIZATION PROCEDURE

We consider the discrete equilibrium equation $\boldsymbol{P}\cdot\boldsymbol{V}_{i+1}+\boldsymbol{Q}\cdot\boldsymbol{V}_i+\boldsymbol{R}\cdot\boldsymbol{V}_{i-1}+\boldsymbol{F}_i=\boldsymbol{0}$ appearing in (2.8) and derive here its continuous equivalent in the outer region. The discrete force and the nodal displacements are replaced by their continuous interpolations, see (2.11) and (4.4) respectively. This yields

$$\begin{aligned}\frac{1}{\varepsilon}\boldsymbol{P}\cdot\left[\begin{pmatrix}u-\varepsilon y\\ u+\varepsilon y\end{pmatrix}+\varepsilon\,\delta\begin{pmatrix}-u'+\varepsilon y'\\ u'+\varepsilon y'\end{pmatrix}+\frac{\varepsilon^2\delta^2}{2}\begin{pmatrix}u''-\varepsilon y''\\ u''+\varepsilon y''\end{pmatrix}+\cdots\right]_{x=\varepsilon(i+1)}\\ +\frac{1}{\varepsilon}\boldsymbol{Q}\cdot\left[\begin{pmatrix}u-\varepsilon y\\ u+\varepsilon y\end{pmatrix}+\varepsilon\,\delta\begin{pmatrix}-u'+\varepsilon y'\\ u'+\varepsilon y'\end{pmatrix}+\frac{\varepsilon^2\delta^2}{2}\begin{pmatrix}u''-\varepsilon y''\\ u''+\varepsilon y''\end{pmatrix}+\cdots\right]_{x=\varepsilon i}\\ +\frac{1}{\varepsilon}\boldsymbol{R}\cdot\left[\begin{pmatrix}u-\varepsilon y\\ u+\varepsilon y\end{pmatrix}+\varepsilon\,\delta\begin{pmatrix}-u'+\varepsilon y'\\ u'+\varepsilon y'\end{pmatrix}+\frac{\varepsilon^2\delta^2}{2}\begin{pmatrix}u''-\varepsilon y''\\ u''+\varepsilon y''\end{pmatrix}+\cdots\right]_{x=\varepsilon(i-1)}\\ +\frac{\varepsilon}{2}\begin{pmatrix}\bar f(\varepsilon\,(i-\delta))\\ \bar f(\varepsilon\,(i+\delta))\end{pmatrix}\;=\;\boldsymbol{0},\end{aligned}$$

where the subscripts ε in u_ε and y_ε are implicit and $\delta=1/4$. Next we Taylor-expand the displacements u_ε and y_ε about $x=\varepsilon i$. Grouping the terms, we can then rewrite the equilibrium as

$$\begin{aligned}k_1\Bigg(&\boldsymbol{T}_0 y_\varepsilon(x)+\varepsilon\boldsymbol{T}_1 y_\varepsilon'(x)+\varepsilon^2\boldsymbol{T}_2 y_\varepsilon''(x)+\varepsilon^3\boldsymbol{T}_3 y_\varepsilon^{(3)}(x)\\ &+\boldsymbol{t}_0 u_\varepsilon'(x)+\varepsilon\boldsymbol{t}_1 u_\varepsilon''(x)+\varepsilon^2\boldsymbol{t}_2 u_\varepsilon^{(3)}(x)+\varepsilon^3\boldsymbol{t}_3 u_\varepsilon^{(4)}(x)\Bigg)\\ &+\frac{1}{2}\left(\varepsilon\bar f(x)\begin{pmatrix}1\\1\end{pmatrix}+\frac{\varepsilon^2}{4}\bar f'(x)\begin{pmatrix}-1\\1\end{pmatrix}+\frac{\varepsilon^3}{32}\bar f''(x)\begin{pmatrix}1\\1\end{pmatrix}\right)\;=\;\mathcal{O}(\varepsilon^4)\end{aligned}\tag{B.1}$$

where $x=\varepsilon i$. The vectors $\boldsymbol{t}_j\in\mathbb{R}^2$ and $\boldsymbol{T}_j\in\mathbb{R}^2$ collect the coefficients of the Taylor expansions and their full expressions in terms of the spring constants $(k_1,\dots,k_4)$ are available in the companion notebook [Thb24]. Table B.1 contains the values of the coefficients $\boldsymbol{t}_j$ and $\boldsymbol{T}_j$ for the particular spring constants listed in Table 2.1.

$\boldsymbol{t}_0$	$\boldsymbol{t}_1$	$\boldsymbol{t}_2$	$\boldsymbol{t}_3$	$\boldsymbol{T}_0$	$\boldsymbol{T}_1$	$\boldsymbol{T}_2$	$\boldsymbol{T}_3$
$\begin{pmatrix}-1\\1\end{pmatrix}$	$\frac{1}{4}\begin{pmatrix}7\\11\end{pmatrix}$	$\frac{1}{96}\begin{pmatrix}-43\\67\end{pmatrix}$	$\frac{1}{384}\begin{pmatrix}59\\103\end{pmatrix}$	$8\begin{pmatrix}1\\-1\end{pmatrix}$	$3\begin{pmatrix}-1\\-1\end{pmatrix}$	$\begin{pmatrix}0\\1\end{pmatrix}$	$\frac{1}{32}\begin{pmatrix}1\\9\end{pmatrix}$

Table B.1. Series coefficients of the equilibrium equations (B.1), for the particular spring constants listed in Table 2.1.